

FOUR ECCENTRIC MERGERS INCREASE THE EVIDENCE THAT LIGO–VIRGO–KAGRA’S BINARY BLACK HOLES FORM DYNAMICALLY

Isobel Romero-Shaw,^{1,2,3} Paul D. Lasky,^{1,2} and Eric Thrane¹

¹*School of Physics and Astronomy, Monash University, Clayton VIC 3800, Australia*

²*OzGrav: The ARC Centre of Excellence for Gravitational Wave Discovery, Clayton VIC 3800, Australia*

³*Department of Applied Mathematics and Theoretical Physics, Cambridge CB3 0WA, United Kingdom*

ABSTRACT

The growing population of compact binary mergers detected with gravitational waves contains multiple events that are challenging to explain through isolated binary evolution. Such events have higher masses than are expected in isolated binaries, component spin-tilt angles that are misaligned, and/or non-negligible orbital eccentricities. We investigate the close-to-merger orbital eccentricities of 62 binary black hole candidates from the third gravitational-wave transient catalogue of the LIGO-Virgo-KAGRA Collaboration, finding that at least four of these events show significant support for eccentricity $e_{10} \geq 0.1$ at a gravitational-wave frequency of 10 Hz. Two of these events are new additions to the population: GW191109 and GW200208_22. If the four eccentric candidates are truly eccentric, our results suggest that densely-populated star clusters may produce 100% of the observed mergers. However, it remains likely that other formation environments with higher yields of eccentric mergers—for example, active galactic nuclei—also contribute. We estimate that we will be able to confidently distinguish which formation channel dominates the eccentric merger rate after $\gtrsim 80$ detections of events with $e_{10} \geq 0.05$ at LIGO–Virgo sensitivity, with only ~ 5 detectably-eccentric events required to distinguish formation channels with third-generation gravitational-wave detectors.

INTRODUCTION

The LIGO-Virgo-KAGRA (LVK) collaboration has so far reported 90 gravitational-wave signals of probable ($\geq 50\%$ credible) astrophysical origin (Abbott et al. 2019; Abbott et al. 2021b,c,a), all consistent with coming the mergers of a compact binary: a binary black hole (BBH), binary neutron star (BNS) or neutron star–black hole binary (NSBH). The provenance of these compact-object binary mergers is an open question in gravitational-wave astrophysics. In order for an isolated pair of stars to merge as a compact binary on an observable timescale, it must undergo specific evolutionary scenarios. Typically, isolated binaries must harden either through Roche-lobe overflow mass transfer (van den Heuvel et al. 2017; Neijssel et al. 2019; Bavera et al. 2020; Olejak et al. 2021; Gallegos-Garcia et al. 2021) or common-envelope evolution (Livio & Soker 1988; Bethe & Brown 1998; Ivanova et al. 2013; Kruckow et al. 2016), or be born with a small enough separation that chemically-homogeneous evolution is possible (e.g., de Mink et al. 2010; de Mink & Mandel 2016; Marchant et al. 2016). Compact objects can instead be driven to merge rapidly by dynamical interactions, which can happen

in populous environments like star clusters (e.g., Rodriguez et al. 2018b,a; Samsing et al. 2018).

The different processes that facilitate the merger of a binary leave their signature on the resulting gravitational-wave signal. Multiple studies have shown how the compact-object masses, spins, and orbital eccentricities inferred from the signal may act as identifiers of different formation scenarios, both for individual events and for the contribution of different formation pathways to the entire population (e.g., Vitale et al. 2017; Stevenson et al. 2015; Gerosa & Berti 2017; Bavera et al. 2020; Mapelli 2020; Sedda et al. 2020; Zevin et al. 2021b). In addition, the redshift evolution of the merger rate should contain distinct contributions from different formation channels (e.g., Mandic et al. 2016; Franciolini et al. 2021), although this will only be resolvable after $O(100)$ detections (Fishbach et al. 2018).

Non-zero orbital eccentricity is arguably the most robust signature of dynamical formation.¹ A binary undergoing isolated evolution is expected to circularise before its

ir346@cam.ac.uk

¹Lidov-Kozai resonant oscillations can drive up the eccentricity of a merging binary in an isolated triple system (Lidov 1962; Kozai 1962; Naoz 2016; Antonini et al. 2017), but the relative contribution of this channel to the observable eccentric merger rate is thought to be low even if optimistically low black-hole natal kicks and metallicities are assumed (Silsbee & Tremaine 2017; Rodriguez & Antonini 2018).

gravitational-wave frequency reaches the start of the LVK frequency band at 10 Hz (Peters 1964). In contrast, dynamically-induced mergers often merge so rapidly that they retain non-negligible orbital eccentricity at 10 Hz, a quantity that we refer to as e_{10} . Robust predictions exist for the distribution of binary eccentricities in dense star clusters (e.g., Samsing 2018; Samsing & Ramirez-Ruiz 2017; Samsing & D’Orazio 2018; Zevin et al. 2019; Rodriguez et al. 2018b,a), with $\sim 5\%$ of mergers in these environments retaining $e_{10} \geq 0.1$. When current detector sensitivities and search method limitations are taken into account, we expect to be able to measure the eccentricities of $\sim 4\%$ of mergers from dense star clusters (Lower et al. 2018; Romero-Shaw et al. 2019; Zevin et al. 2021a).² Expectations from galactic nuclei and active galactic nuclei (AGN) disks are also becoming clearer, with up to 70% of mergers in AGN disks thought to retain $e_{10} \geq 0.1$ (e.g. Samsing et al. 2020; Tagawa et al. 2021b; Gondán & Kocsis 2021; Vajpeyi et al. 2021).

Although non-zero orbital eccentricity is one calling card of dynamical formation, the component masses of a compact-object merger may also help to distinguish its origins. While pair-instability supernovae prevent black holes forming between around ~ 60 and $\sim 130 M_{\odot}$ in isolation (Heger & Woosley 2002; Belczynski et al. 2016; Marchant et al. 2016; Woosley 2017; Fishbach & Holz 2017), dynamical environments can build massive black holes through hierarchical mergers or accretion (e.g., Fishbach et al. 2017; Rodriguez et al. 2019; Gerosa & Berti 2019; Anagnostou et al. 2020; Kimball et al. 2020; Kremer et al. 2020a; Samsing & Hotokezaka 2020; Gerosa & Fishbach 2021; Banerjee 2021; Zevin & Holz 2022). Nonetheless, the uncertain limits and range of the pair-instability mass gap (Sakstein et al. 2020; Belczynski 2020; Farmer et al. 2019; Woosley & Heger 2021; Ziegler & Freese 2021) reduce the efficacy of compact-object mass as an identifier of formation channel.

The spin *directions* of a binary’s components can indicate its formation mechanism (Farr et al. 2017; Stevenson et al. 2017; Talbot & Thrane 2017). Isolated binaries are expected to have spins approximately aligned with the binary angular momentum vector (e.g., Campanelli et al. 2006; O’Shaughnessy et al. 2017; Gerosa et al. 2018; Kalogera 2000), while dynamically-assembled pairs in spherically-symmetric environments should have an isotropic distribution of relative spin tilts (e.g., Rodriguez et al. 2016). However, mergers with aligned spins are not necessarily of isolated ori-

gin: gas torques in AGN disks can align component spins (Bogdanović et al. 2007) if the timescale for dynamical interaction is sufficiently long (Liu & Lai 2017; Tagawa et al. 2020), and dynamically-assembled binaries in open clusters can have aligned spins because few dynamical encounters can occur before merger (Trani et al. 2021).

Black hole spin *magnitudes*, too, can distinguish binary formation mechanisms. Merger products should develop high spins as they accumulate angular momentum through repeated mergers, so high spin magnitude can indicate dynamical formation (Fishbach et al. 2017; Kimball et al. 2020; Tagawa et al. 2021a), since the spins of black holes that form via stellar collapse are typically expected to be small. However, chemically homogeneous evolution (Marchant et al. 2016; Mandel & de Mink 2016; Qin et al. 2019), mass transfer and/or tidal locking in tight binaries (Valsecchi et al. 2010; Qin et al. 2019; Neijssel et al. 2021; Izzard et al. 2003; Belczynski et al. 2020; Bavera et al. 2020; Zevin & Bavera 2022; Broekgaarden et al. 2022), and differential rotation between the stellar core and envelope (Hirschi et al. 2005) can also produce rapidly-spinning black holes.

In addition to those proceeding via isolated evolution or dynamical formation, mergers can also occur between primordial black holes that form through direct collapse of density fluctuations in the early Universe. While primordial black holes can have masses and spins that mimic those of isolated or dynamical black holes, with no upper or lower mass limit and preferentially zero spin (unless spun-up by accretion over the majority of cosmic history), primordial mergers should have zero eccentricity at detection (Green & Kavanagh 2021; Franciolini et al. 2021). Non-zero orbital eccentricity is also, therefore, a reliable way to rule out the primordial binary hypothesis.

Within the growing population of LVK observations are events that are challenging to explain through isolated stellar evolution. The first event to breach the pair-instability mass gap at $\geq 90\%$ confidence was GW190521 (Abbott et al. 2020), which also exhibited signs of spin-induced precession and/or orbital eccentricity greater than 0.1 at 10 Hz (Romero-Shaw et al. 2020b; Gayathri et al. 2022; Calderón Bustillo et al. 2021). A second binary black hole merger, GW190620, also supports a dynamical formation hypothesis, with $e_{10} \geq 0.05$ at 74% credibility (Romero-Shaw et al. 2021a). New events that support the dynamical formation hypothesis have emerged in GWTC-2.1 and GWTC-3. These include additional upper mass-gap events, such as GW190426_19 (Abbott et al. 2021c) and GW200220_06 (Abbott et al. 2021a), and events consistent with having negatively-aligned or substantially misaligned component spins, such as GW191109 and GW200129 (Abbott et al.

²Existing detectors have been shown to be sensitive to eccentricities $e_{10} \gtrsim 0.05$ for BBH mergers (Lower et al. 2018; Romero-Shaw et al. 2019). Signal detection currently depends on achieving a high signal-to-noise ratio between the data and a quasi-circular signal template, so eccentric signals have reduced detectability compared to quasi-circular signals. Roughly half of the $\sim 7\%$ of mergers in dense star clusters with $e_{10} \geq 0.05$ will be recoverable with such a search (Zevin et al. 2021a).

2021a; Hannam et al. 2021).³ On top of these individual-event clues, population-level hints of dynamical formation come from evidence for hierarchical mergers (Kimball et al. 2021) and the mass-gap-encroaching shape of the inferred mass distribution. Hints of misaligned spins (negative effective spin parameter χ_{eff}) have been claimed at the population level (Abbott et al. 2021d); some follow-up studies show that the population is consistent with the majority of binaries having non-zero and misaligned component spins, while others argue that the population is consistent with a majority of binaries having $\chi_{\text{eff}} = 0$ and only a small subset having significant positive χ_{eff} (Roulet et al. 2021; Galaudage et al. 2021).

Eccentricity is not included in the gravitational-waveform models used by the LVK to produce the inferences reported in their catalogues, because incorporating the effects of eccentricity makes physically-accurate waveform models too slow for conventional inference methods. In Romero-Shaw et al. (2019, 2020a,b, 2021a), we used an efficient reweighting method to obtain measurements of the orbital eccentricity of gravitational-wave sources up to and including the second LVK gravitational-wave transient catalogue, GWTC-2. In this work, we use the same method to analyse additional binary black hole candidates from the most recent catalogues of LVK events: the updated second catalogue, GWTC-2.1, and the third catalogue, GWTC-3. We report an additional two binaries with significant support for $e_{10} \geq 0.05$, adding to the building evidence for a dynamically-formed subset within the observed mergers.

This paper is structured as follows. In Section 2 we describe our methodology, and note its limitations. In Section 3 we present results from our analysis of new events from GWTC-2.1 and GWTC-3, taking the total number of BBH candidates investigated for signatures of eccentricity to 62. Two events, GW191109 and GW200208_22, have $\geq 70\%$ of their posterior support at $e_{10} \geq 0.05$ and have inconclusive but positive log Bayes factors in favour of the eccentric hypothesis, with $\ln \mathcal{B}(e_{10} \geq 0.05) \gtrsim 1.4$. We present analyses of eccentricity at the population level in Section 4, and demonstrate that $\gtrsim 80$ detectably-eccentric mergers are required to confidently distinguish different dynamical formation scenarios at current detector sensitivity. In Section 5, we conclude with some final thoughts. Results for events with negligible eccentricity are provided in Appendix A.

METHOD

We use a reweighting method (see Payne et al. 2019; Romero-Shaw et al. 2019) to efficiently calculate poste-

rior probability distributions using the aligned-spin eccentric waveform model SEOBNRE (Cao & Han 2017). First, we run an importance-sampling step, performing Bayesian inference using bilby and the bilby_pipe pipeline (Ashton et al. 2019; Romero-Shaw et al. 2020c). We run five parallel analyses with unique seeds for each event with the dynesty sampler (Speagle 2019), utilising spin-aligned quasi-circular model IMRPhenomD (Khan et al. 2016) as the ‘proposal’ model. For these initial analyses, we use 1000 live points, 100 walks and 10 auto-correlation times. For follow-up analyses on eccentric candidates, we use 4000 live points and 200 walks. We use a sampling rate of 4096 Hz and a reference frequency of 10 Hz for every event.

We reweight the proposal samples obtained in the initial step to our ‘target’ model: SEOBNRE, a spin-aligned eccentric waveform approximant containing the inspiral, merger and ringdown sections of the signal. Since this is a time-domain model, we use a Fourier transform to obtain frequency-domain waveforms for use in the likelihood, softening the abrupt start of the time-domain inspiral using a half-Tukey window to avoid spectral leakage. We analyse publicly-available data from GWTC-2.1 and GWTC-3 (Abbott et al. 2021c,a; Abbott et al. 2021a,b) and use detector noise curves generated using BayesWave (Cornish & Littenberg 2015; Littenberg & Cornish 2015).

We use standard priors on right ascension α , declination δ , source inclination θ_{JN} , polarisation ϕ , coalescence phase ψ and geocent time t_0 . Our prior on mass ratio q is uniform between 0.125 and 1, and our priors on the aligned component spin magnitudes χ_1, χ_2 are capped at the SEOBNRE maximum of ± 0.6 . We use uniform priors on chirp mass \mathcal{M} and priors on luminosity distance d_L that are uniform in the source frame. We marginalise over phase and coalescence time to mitigate definitional differences between the two models.

Including all events in GWTC-3, we report results for 62 BBH candidates in total. We reserve detailed analyses of other events, including binaries that contain neutron stars, for future work.⁴ The events that we do *not* discuss in this work are:

- **Events for which the reweighting process failed to achieve an adequate effective sample size.** The number of effective samples in a posterior distribution after reweighting is

$$n_{\text{eff}} = \frac{(\sum_{i=1}^n w_i)^2}{\sum_{i=1}^n w_i^2}. \quad (1)$$

We deem any events with $n_{\text{eff}} < 100$ undersampled, and do not include them in the main body of this

³The strength of the support for anti-aligned or misaligned spins in GW200129 and GW191109 is contested by Payne et al. (2022) and Tong et al. in prep., respectively, who show that this support may be highly dependent on the data cleaning methods used.

⁴BNS mergers have so far been found to be consistent with quasi-circularity (Romero-Shaw et al. 2020a; Lenon et al. 2020)

work. The undersampled events from GWTC-2.1 and GWTC-3 are listed along with undersampled events from GWTC-2 in Appendix B.

- **Binaries likely to contain at least one neutron star.**

These include those confidently designated as binary neutron stars (BNS; GW170817, GW190425), neutron star–black hole (NSBH) binaries (GW191219, GW200105, GW200115), and events with secondaries of ambiguous mass that may be black holes or neutron stars (GW190814, GW190917, GW200210). We neglect BNS and likely NSBH events from the analysis presented in the main body of this paper because their formation mechanisms may be drastically different from those of BBH mergers, and we wish to make statements about the formation channels that produce the BBH mergers in our population. When studied with the reweighting method, we find that GW190814A fails to achieve a high reweighting efficiency; this is expected, since higher-order modes are known to be present in this signal, and both models used in this work incorporate only the (2, 2) mode (Abbott et al. 2020). GW190412, which is thought to be a unequal-mass black hole binary with mass ratio $q \sim 0.27$, also has higher-order mode content, and also ends up undersampled (see Appendix B). We provide posterior probability distributions for ambiguous binaries GW190917 and GW200210 in Appendix C. The eccentricity distribution inferred for both events is uninformative.

Caveats

Our analysis method leads our results to have the following caveats:

1. Since the waveform model that we employ, SEOBNRE, does not support misaligned spins, we are not able to disentangle the effects of orbital eccentricity and spin-induced precession on the signal. This may lead us to infer non-zero eccentricity for a quasi-circular system undergoing spin-precession; see Romero-Shaw et al. (2020b).
2. SEOBNRE enforces a dimensionless aligned-spin magnitude upper limit of 0.6. Any binary that is truly highly-spinning will produce a signal that is poorly-specified by our choice of waveform model, and will therefore bias our results.
3. Similarly, the upper limit of our eccentricity prior is 0.2 at a detector-frame gravitational-wave frequency of 10 Hz. Any binary with an eccentricity higher than this will not be correctly specified by our choice of waveform model. However, we have seen in the case of

GW190521 that systems consistent with larger eccentricities (Calderón Bustillo et al. 2020; Gayathri et al. 2022) will still show signs of high eccentricity in our analyses, railing against the model-enforced upper limit of the prior (see, e.g., Romero-Shaw et al. 2020b).

4. SEOBNRE sets the initial argument of periapsis based on the fixed starting frequency of waveform generation. This parameter is therefore not adjustable and cannot be sampled over. We anticipate that being able to sample over this parameter could lead to a shift in the locations of the peaks of the recovered eccentricity distributions in events with high signal-to-noise ratio ($\text{SNR} \approx 30$), but the consequences of neglecting this parameter for the events studied here are likely to be small (Clarke et al. 2022).
5. Different waveform models and simulations use different definitions of eccentricity, and use different prescriptions to set initial conditions. This means that an eccentricity inferred with SEOBNRE does not exactly equate to the eccentricity that would be inferred with another model, and that comparisons to predictions made by simulations of dynamical environments should be taken as indicative rather than absolute. Work is ongoing to establish a translation guide between the eccentricities defined by various simulations (Knee et al. 2022, in prep.).
6. We restrict our analyses to events that have been flagged as likely compact binary merger signals by LVK searches. In order to be flagged as such, a signal must bear significant resemblance to a quasi-circular inspiral track so that it achieves a high match with the waveforms used in those templated searches. As a result, the events we analyse are highly likely to have small or negligible eccentricities.

ECCENTRICITY MEASUREMENTS

In Figure 1, we provide marginal one-dimensional eccentricity posterior distributions for 62 BBH candidates. We note that we have removed two events that were found to have below-threshold significance in GWTC-2.1 (GW190924A and GW190909A; Abbott et al. 2021c), from this plot and from all analyses presented in Section 4. We present in Figure 2 marginal posteriors on $\log_{10}(e_{10})$ for the ten analysed events in GWTC-2.1 and GWTC-3 that have positive log Bayes factors in favour of the eccentric hypothesis when compared to the quasi-circular hypothesis. Posterior probability distributions on all parameters of all analysed events are provided online.⁵

⁵github.com/IsobelMarguarethe/eccentric-GWTC-3

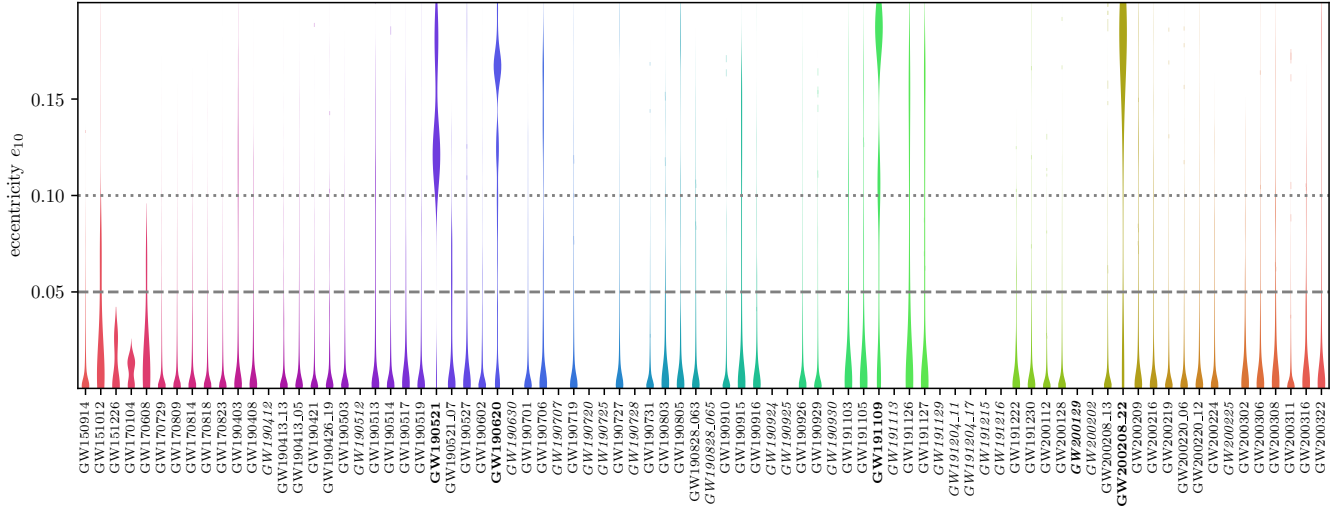


Figure 1. Marginal posterior distributions on e_{10} for all adequately-sampled binary black hole merger events in GWTC-3 are shown in colour. The width of the violin at each value of eccentricity is proportional to the posterior distribution at that value. The names of undersampled events are italicised and their posteriors are not shown. The names of the four events that show considerable support for $e_{10} \geq 0.05$ are emboldened.

Table 1. A summary of the detector-frame eccentricity measurements for events in GWTC-3 with a log Bayes factor greater than 0 for the hypothesis that $e_{10} \geq 0.05$ and number of effective samples ≥ 100 . The two events with greater than 50% of their posterior support at $e_{10} \geq 0.05$ are emboldened. The second and third columns provide the percentage of posterior support for $e_{10} > 0.1$ and $e > 0.05$, two values typically used as thresholds for currently detectable binary eccentricity at 10 Hz. However, these values are somewhat arbitrary, as each individual signal has a different detectable eccentricity threshold. Furthermore, simulations that quote eccentricity $e_{10} \geq 0.1$ do so in the source frame; one must redshift any detector-frame eccentricity measurements to perform a direct comparison to such simulations (see Section 4). The third (fourth) column provides the natural log Bayes factor for the hypotheses that $e_{10} \geq 0.1$ (0.05) against the hypothesis that $e_{10} < 0.1$ (0.05). The final column states the number of effective samples in the eccentric posterior after reweighting. The quantities presented in this table are provided for events in GWTC-3 without significant support for eccentricity in the Appendix in Tables 3 and 4.

Event name	$e_{10} \geq 0.1$ (%)	$e_{10} \geq 0.05$ (%)	$\ln \mathcal{B}(e_{10} \geq 0.1)$	$\ln \mathcal{B}(e_{10} \geq 0.05)$	n_{eff}
GW190403	16.64	27.53	0.83	0.56	6358
GW190805	14.33	23.78	0.19	0.03	719
GW191105	10.58	18.52	0.29	0.12	718
GW191109	62.52	71.53	1.89	1.49	7125
GW191126	26.28	33.79	1.27	0.92	293
GW191127	23.68	33.33	1.20	0.88	436
GW200208_22	70.78	73.06	1.94	1.39	219
GW200209	16.58	26.63	0.64	0.44	43848
GW200216	10.62	22.43	0.26	0.25	3108
GW200322	12.57	21.37	0.12	0.07	10203

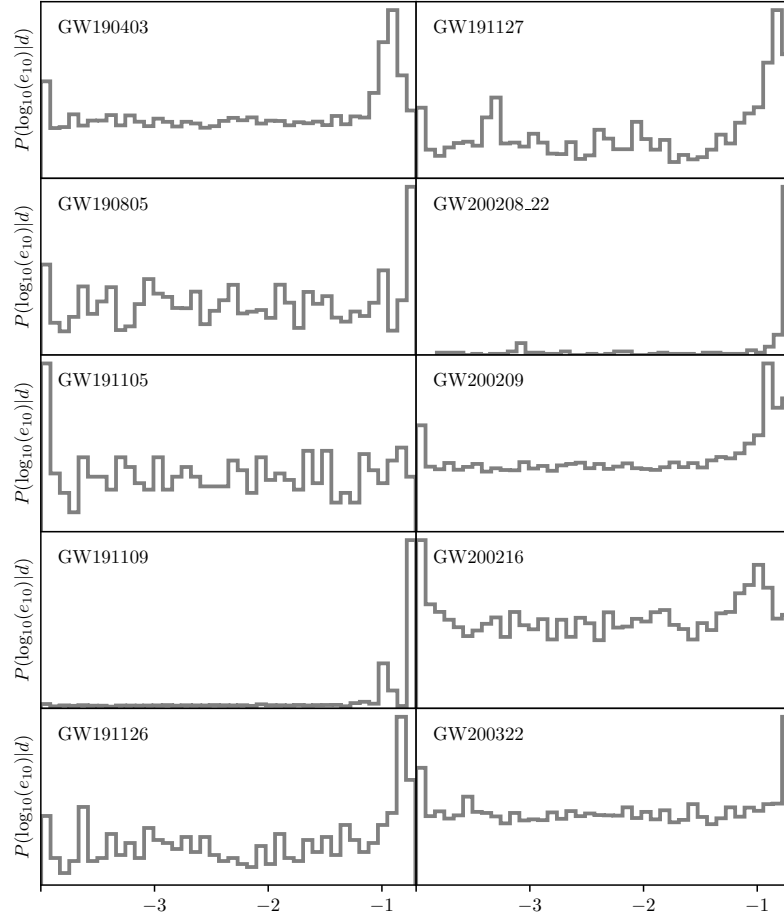


Figure 2. Marginal posterior distributions on $\log_{10}(e_{10})$ for events highlighted in Table 1, which have a significant fraction of their posterior support above $e_{10} = 0.05$ and a positive log Bayes factor when comparing the eccentric hypothesis to the quasi-circular hypothesis. We label each panel with the name of the event.

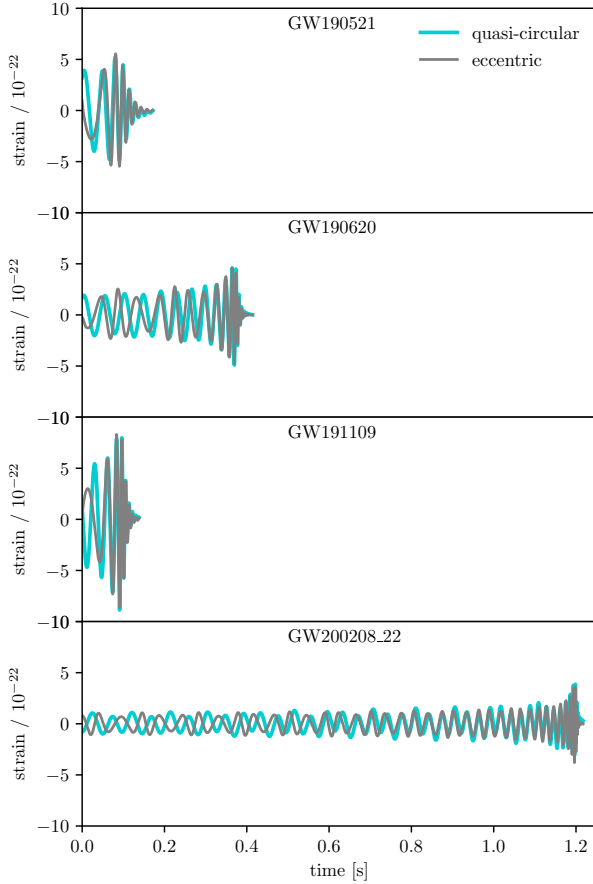


Figure 3. Time-domain waveforms for the median posterior parameters inferred for the four events with support for $e_{10} \geq 0.05$ observed by the LIGO and Virgo detectors so far. The preferred SEOBNRE waveforms are shown in grey and the corresponding quasi-circular IMRPhenomD waveforms are shown in teal. The panel width spans 1.25 seconds.

Events from GWTC-3 with majority support for $e_{10} \geq 0.05$

There are two new events that show significant evidence for eccentricities above $e_{10} = 0.05$, with $\geq 50\%$ of their posterior probability support above $e_{10} = 0.05$. For these events, and for the two eccentric candidates GW190521 and GW190620 (Romero-Shaw et al. 2020b, 2021a), we conduct our analysis with more aggressive sampler settings (4000 live points and 200 walks) to obtain a higher number of effective samples. These results are those shown in Fig. 1 and all other figures, and in Table 1. The waveforms corresponding to the median posterior parameters for GW190521, GW190620, GW191109 and GW200208 are shown in Fig. 3.

GW191109

GW191109 was found by the LVK analysis to have the highest support for negative spin of all GWTC-3 events. Our initial quasi-circular analysis recovers this preference for negatively-aligned spins, but when we reweight to the eccentric posterior,

higher spin magnitudes have lower weights. This is similar to the reweighting behaviour observed for eccentric candidate GW190620 (Romero-Shaw et al. 2021a), although we retain some appreciable deviation from the spin prior for χ_1 after reweighting for GW191109. Other parameters are consistent with those recovered in the LVK analysis. Proposal (quasi-circular) posteriors for GW191109 are shown in Fig. 4 in teal, and target (eccentric) posteriors are overplotted in grey.

We find that GW191109 has 72.19% of its posterior support above $e_{10} = 0.05$, 62.63% of its posterior above $e_{10} = 0.1$, and a log Bayes factor of $\ln \mathcal{B} = 1.49$ (1.89) in favour of the $e_{10} \geq 0.05$ ($e_{10} \geq 0.1$) hypothesis relative to the quasi-circular hypothesis. For this event, we obtain a reweighting efficiency of 4.52%, and obtain $n_{\text{eff}} = 7125$. Visible in Figure 1 is the double-peaked structure of the eccentricity posterior for GW191109: the main peak is at the upper limit of the eccentricity prior, $e_{10} = 0.2$, but there is a subdominant mode at $e_{10} \approx 0.1$.

The eccentric (target) posterior distribution on the phase of coalescence, ϕ , for GW191109 has periodic peaks that are not present in the quasi-circular (proposal) posterior distribution. This implies that eccentricity can increase the measurability of ϕ . Since GW191109 is relatively high-mass, its e_{10} measurement gives the shape of its orbit just a few cycles before the coalescence itself. Having distinctly non-zero orbital eccentricity at this point means that the orbit close-to-merger is elongated, so the gravitational-wave emission varies more strongly with ϕ , making it easier to constrain.

GW200208_22

We find that, when analysed with our default sampling settings, the mass ratio posterior for GW200208_22 rails against the lower limit of the prior. Therefore, for this event, we reduce the lower mass ratio prior limit from 0.125 to 0.025. We notice also that the posterior rails against the upper limits of χ_1 and χ_2 at 0.6. However, since this is a limit enforced by SEOBNRE, we do not relax this limit. In Fig. 5, we show proposal (quasi-circular) posteriors for GW200208_22 in teal and target (eccentric) posteriors in grey.

We find that GW200208_22 has 76.71% of its posterior support above $e_{10} = 0.05$, with 73.52% above $e_{10} = 0.1$, and log Bayes factor for $e_{10} \geq 0.05$ ($e_{10} \geq 0.1$) relative to the quasi-circular hypothesis of 1.45 (1.92). In our analysis, GW200208_22 has a source-frame chirp mass of $17.38^{+3.10}_{-4.54} M_{\odot}$. The reweighting efficiency for GW200208_22 is relatively low at 0.18%, consistent with our expectations for low-chirp mass (long-duration) eccentric signals. Additionally, waveform model choice been shown to be important for this event (Abbott et al. 2021a), so posterior differences that are not correlated with eccentricity may be a result of waveform systematics. We obtain 219 effective samples for this event.

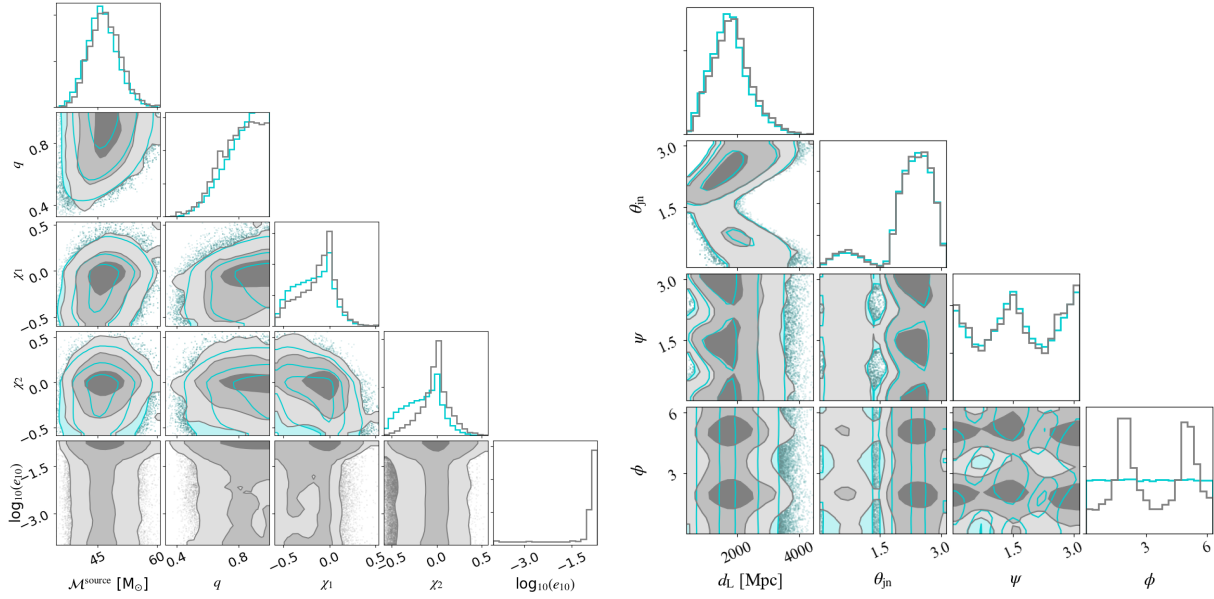


Figure 4. Intrinsic (left) and extrinsic (right) parameters inferred for GW191109. Posterior probability distributions under the eccentric model are shown in grey, while the underlying quasi-circular posteriors used to importance-sample the parameter space are shown in teal.

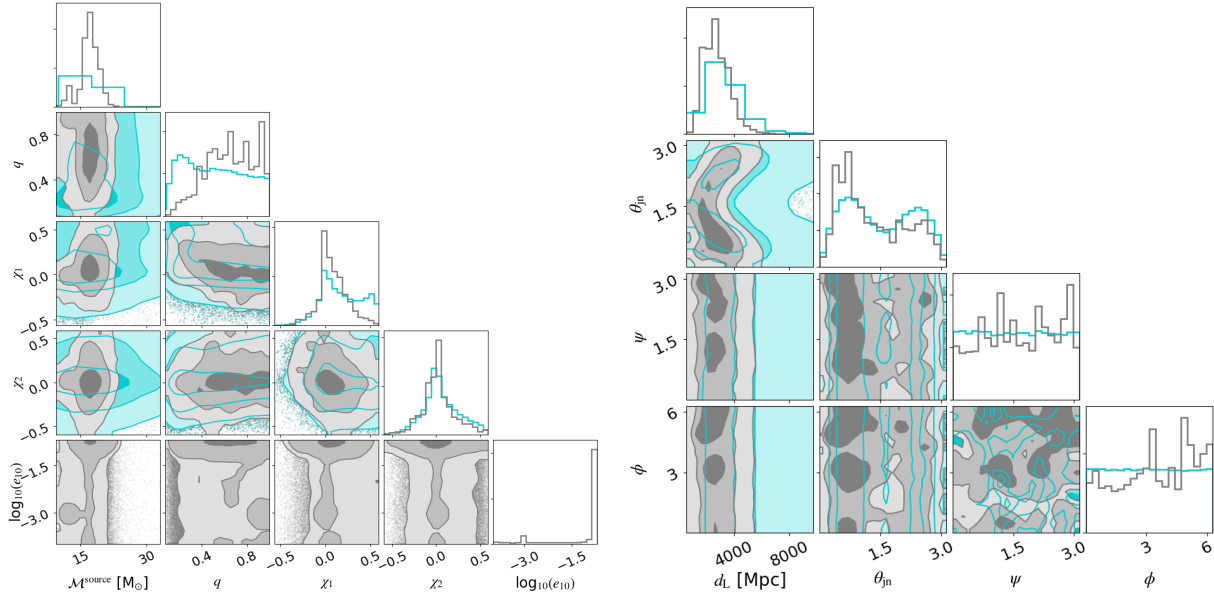


Figure 5. Intrinsic (left) and extrinsic (right) parameters inferred for GW200208_22.

Our posteriors peak at a lower total mass ($\sim 41 M_{\odot}$) than that found in the LVK analysis ($\sim 63 M_{\odot}$), although the posteriors do overlap: while the LVK posteriors and our IMRPhenomD posteriors are multimodal, the eccentric posterior favours the lower-mass peak. The median primary mass recovered with the eccentric model ($\sim 25 M_{\odot}$) is significantly lighter than the median of the LVK analysis ($\sim 51 M_{\odot}$), for the same reason. As a result, the median luminosity distance recovered is roughly 1 Gpc smaller than the median LVK result. It is possible for eccentric systems to masquerade as

higher-mass quasi-circular systems when their gravitational-wave signals are analysed assuming quasi-circularity, since eccentricity can drive a binary to merge on a faster timescale and merge at a lower frequency (see, e.g., [Calderón Bustillo et al. 2020](#); [Favata et al. 2022](#)). In addition to the inclusion of eccentricity, another reason for the discrepancy in median posterior parameters may be our enforced limit on the spin prior magnitude due to the limitations of SEOBNRE: while the LVK analysis finds that $\chi_1 \geq 0.29$ (90% credibility) with

51% of its posterior support above $\chi_1 = 0.8$, our posterior rails against the upper limit of the prior at $\chi_1 = 0.6$.

As in the LVK analysis, the mass ratio posterior recovered with IMRPhenomD is quite flat, with a slight preference for unequal masses ($m_2/m_1 \approx 0.3$). When we reweight to SEOBNRE, the long tail out to high masses is downweighted and only the peak at chirp mass $\mathcal{M} \approx 16 M_\odot$ remains. More equal mass ratios are favoured by the eccentric model over unequal masses. Higher values of χ_1 and χ_2 are also downweighted, with the eccentric model preferring samples with high values of eccentricity and low values of spin. Again, the reason for the difference may be the enforced spin prior limitation. It is possible that the data is best-fit by a waveform with $\chi_1 \sim 0.9$ and $e_{10} = 0$, but prefers a waveform with $\chi_1 = 0$ and $e_{10} = 0.2$ to one with $\chi_1 \sim 0.5$. In this case, because of our restricted prior, the vast majority of the eccentric posterior is at high eccentricities with low spins. Previous analyses have shown that, when spin amplitude is restricted, higher eccentricities may be favoured (see O’Shea & Kumar 2021)

Other events in GWTC-3 with non-negligible support for $e_{10} \geq 0.05$

Another two candidates from O3b, GW191126 and GW191127, have $> 30\%$ of their posterior support at $e_{10} \geq 0.05$ and $\ln \mathcal{B}(e_{10} \geq 0.1) > 1.0$. Their marginal eccentricity posterior distributions show peaks at our prior upper limit of $e_{10} = 0.2$ and non-negligible tails down to lower eccentricities. While we also analyse these event with more aggressive sampler settings, we do not discuss these events in detail here; we reserve a detailed analysis of these events, in conjunction with the marginal eccentric candidates presented in Romero-Shaw et al. (2021a), for future work.

Notable events in GWTC-3 with $e_{10} \leq 0.05$

Mass-gap events

GW191109 and GW200208_22 are both highlighted in Abbott et al. (2021a) as potential events of interest from the perspective of searches for intermediate-mass black holes. GW190426_19 has the highest mass of all binary mergers reported by the LVK, with both components more massive than predicted by isolated evolution: $m_1 = 106.9^{+41.6}_{-25.2} M_\odot$, $m_2 = 76.6^{+26.2}_{-33.6} M_\odot$ (Abbott et al. 2021c). Our analysis of GW190426_19 recovers parameters consistent with those recovered in the LVK analysis, including the slight deviation from the prior at higher values of χ_{eff} . Another high-mass event, GW200220_06, is found by the LVK to have mass-gap components: $m_1 = 87^{+40}_{-23} M_\odot$, $m_2 = 61^{+26}_{-25} M_\odot$ (Abbott et al. 2021a), consistent with our findings. We find that GW190426_19 and GW200220_06 do *not* contain hints of orbital eccentricity.

GW190426_19 and GW200220_06 have high reweighting efficiencies of 72% and 83% respectively, with 11% and 13% of their posterior support above $e_{10} = 0.05$. Reweighting to SEOBNRE pushes the preferred mass-ratio and source-frame chirp mass to slightly lower values for GW190426B, but this shift does not appear correlated with eccentricity; we put the difference down to waveform systematics. There is virtually no difference between the quasi-circular and eccentric posteriors for GW200220_06.

Being consistent with quasi-circular at 10 Hz does not mean that these binaries are not dynamically formed: we expect only $\sim 4\%$ of our detected mergers from globular clusters to retain detectable eccentricity at this frequency (Zevin et al. 2021a), and more massive mergers circularise at lower frequencies than their lower-mass counterparts. It is nonetheless worth noting that the eccentricity, spin magnitude, and spin-tilt measurements for these systems are inconclusive. If they contained merger remnants, which became bound through dynamical interactions, their dimensionless spin magnitudes should be $\chi_i \sim 0.7$, and their spin tilt angles would likely be misaligned (e.g., Pretorius 2005; González et al. 2007; Buonanno et al. 2008). Alternatively, such massive binaries may form in isolation if the pair-instability mass gap is narrower than predicted (as suggested in the wake of GW190521 by, e.g., Costa et al. 2021), or if our standard priors on mass ratio are misleading inference (also suggested to explain GW190521 by Fishbach & Holz 2020).

Spinning events

A number of the events that strongly support nonzero spins are undersampled after the reweighting process: GW200129, which exhibits support for signs of spin-induced precession, GW191204, which has a χ_{eff} posterior tightly constrained away from zero, and GW191216, which has negligible support for $\chi_{\text{eff}} = 0$ (Abbott et al. 2021a). However, some are adequately-sampled: GW191103, for example, which has 175 samples after reweighting. The marginal eccentricity posterior for this event is uninformative, and correlated with spin: lower magnitudes of χ_1 are favoured for samples with $e_{10} \geq 0.05$. The eccentric reweighting process disfavors larger values of χ_1 , while the marginal χ_2 posterior is relatively unchanged. GW191103A has only 17% of its posterior support above $e_{10} = 0.05$ after reweighting.

Spin-induced precession or eccentricity?

There are currently no waveform models that incorporate the simultaneous effects of eccentricity and spin-induced precession on the signal. Since the two effects can cause similar phase and amplitude modulations in gravitational-wave signals (e.g., Calderón Bustillo et al. 2020), they can cause spin-aligned analyses to recover eccentricity, or quasi-circular analyses to recover misaligned spins (Calderón Bustillo et al. 2021; Romero-Shaw et al. 2020b). Therefore, any non-zero

Event	$\ln \mathcal{B}_{E/P}(e_{10} \geq 0.1)$	$\ln \mathcal{B}_{E/P}(e_{10} \geq 0.05)$
GW190521	3.06	2.30
GW190620	2.52	2.10
GW191109	-1.74	-2.14
GW200208_22	1.51	0.96

Table 2. Natural log Bayes factors for the eccentric, spin-aligned hypothesis calculated with waveform model SEOBNRE compared to the quasi-circular, spin-precessing hypothesis calculated with waveform model IMRPhenomXPHM for three potentially-eccentric sources (for an extensive analysis of GW190521 with other spin-precessing approximants, see Romero-Shaw et al. (2020b)). We compare hypotheses for astrophysically-motivated regions of the prior space: above $e_{10} = 0.1$, a common threshold given in the literature, and above $e_{10} = 0.05$, the approximate sensitivity limit for current detectors (Lower et al. 2018; Romero-Shaw et al. 2019, 2021a). In no event is the eccentric hypothesis strongly preferred over the spin-precessing hypothesis, or vice versa.

eccentricity measurements that we infer in our analysis may, in actuality, be caused by the binary having misaligned spins.

Whilst we cannot simultaneously infer the presence of spin-induced precession and eccentricity, we can attempt to deduce which effect is more likely to be present in the signal. We perform analyses on GW190521, GW190620, GW191109 and GW200208_22 using a precessing waveform approximant; see Romero-Shaw et al. (2020b) for an extensive comparison between the eccentric and spin-precessing hypotheses for GW190521. For the study presented here, we employ one of the preferred waveforms used in the transient catalogues of the LVK (Abbott et al. 2021b,c,a): quasi-circular spin-precessing model IMRPhenomXPHM (Pratten et al. 2021), allowing the full range of available spin orientations in our priors and component spin magnitudes up to 0.89, and using the same aggressive sampler settings as employed for our follow-up analyses using SEOBNRE.

Table 2 contains the relative natural log Bayes factors of the spin-aligned, eccentric hypothesis (calculated from our SEOBNRE posteriors above thresholds of $e_{10} = 0.05$ and 0.1) against the quasi-circular, spin-precessing hypothesis (calculated from our IMRPhenomXPHM posteriors) for GW190521, GW190620, GW191109 and GW200208_22. There is a marginal preference for the eccentric hypothesis for GW190521, GW190620, and GW200208_22, and a marginal preference for the spin-precessing hypothesis for GW191109; however, in no case is the evidence for either hypothesis overwhelming. Thus, each one of our potentially-eccentric candidates *could* be eccentric, spin-precessing, or both.

ECCENTRICITY IN THE POPULATION

As the catalogue of mergers grows, it becomes increasingly likely that random noise fluctuations emulate the effects of eccentricity in a subset of BBH merger signals. Additionally,

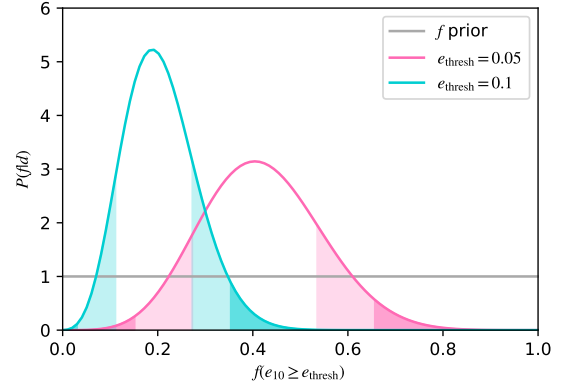


Figure 6. Posterior probability distributions for the fraction of eccentric mergers above $e_{\text{thresh}} = 0.05$ and 0.1 at 10 Hz. The distributions peak at 0.19 (teal curve, representing $e_{\text{thresh}} = 0.1$) and 0.40 (pink curve, representing $e_{\text{thresh}} = 0.05$). The uniform f prior is indicated with a grey horizontal line. Unfilled, lightly-filled and darkest-filled areas represent the symmetric 1σ , 2σ and 3σ credible ranges, respectively. The $f(e_{10} \geq 0.05) = 0$ and $f(e_{10} \geq 0.1) = 0$ points are excluded at greater than 2σ . The $f(e_{10} \geq 0.05) = 0$ point is outside of the symmetric 3σ credible region.

while we highlight four events that have clear peaks above $e_{10} = 0.05$ in their eccentricity posterior probability distributions, there are multiple other events that show significant support for $e_{10} \geq 0.05$. We wish to quantify the fraction of observed mergers that truly support the eccentric merger hypothesis, without assuming any specific formation channel. We perform population analyses under the hypothesis that some binaries have some support for eccentricity e_{10} above some threshold eccentricity, e_{thresh} . We consider two possibilities: that $e_{\text{thresh}} = 0.05$ and that any eccentricity lower than this is not detectable; and a more conservative hypothesis with $e_{\text{thresh}} = 0.1$. We calculate a likelihood for f , the fraction of the population support for $e_{10} \geq e_{\text{thresh}}$:

$$\mathcal{L}(d|f) = \prod_k \left(f \int_{e_{\text{thresh}}}^{e_{\text{max}}} de \pi(e) \mathcal{L}(d_k|e) + (1-f) \int_{e_{\text{min}}}^{e_{\text{thresh}}} de \pi(e) \mathcal{L}(d_k|e) \right). \quad (2)$$

Here, k represents each event in our population, e_{min} and e_{max} are our eccentricity prior bounds, and $\pi(e) \mathcal{L}(d_k|e)$ is the marginal posterior probability distribution for the eccentricity of event k . Drawing proposals for the value of f from a uniform prior and computing $\mathcal{L}(d|f)$ over this range produces a posterior probability distribution for f . This posterior is plotted in Figure 6 for both e_{thresh} conditions.

The highest-probability f representing the fraction of observed BBH with $e_{10} \geq 0.05$ is 0.40, corresponding to 25 mergers, while the maximum-posterior f for BBH observed

with $e_{10} \geq 0.1$ is 0.19, corresponding to 12 mergers. We can exclude $f = 0$ with greater than 2σ credibility in both cases. We therefore conclude that the population support for eccentricity in GWTC-3 is consistent with a non-negligible fraction of mergers exhibiting detectable eccentricity at 10 Hz.

Implications for population formation channels

Simulations suggest that 5–10% of BBH mergers in dense star clusters should enter the LVK sensitivity band with $e_{10} \geq 0.05$ (see, e.g., Samsing 2018; Samsing et al. 2018; Zevin et al. 2019; Rodriguez et al. 2018b,a; Rodriguez et al. 2019; Kremer et al. 2020b). Zevin et al. (2021a) showed that, from a simulated population of mergers from the CMC Cluster Catalog (Kremer et al. 2020b), only 4% of globular cluster mergers could be detected with $e_{10} \geq 0.05$: since gravitational-wave signals from compact binary mergers are detected using search methods that assume quasi-circular inspirals, we expect to detect only 56% of sources with $e_{10} \geq 0.05$. This fraction was calculated using a different eccentric waveform model, TEOBResumS (Nagar et al. 2018), which uses a slightly different definition of reference frequency than SEOBNRE. However, since the overlap between the two waveforms is $O > 90\%$ in LVK noise (see Knee et al. 2022, in prep.), corresponding to a signal-to-noise ratio difference of $\rho = \sqrt{1/O} \lesssim 1$, we assume in this paper that the results of Zevin et al. (2021a) are robust to waveform choice.

Eccentricity distributions obtained from simulations of dense star clusters are naturally quoted at a reference frequency of 10 Hz in the source frame, while we measure eccentricity at a reference frequency of 10 Hz in the detector frame. Since redshifting pushes detector-frame frequencies lower than their source-frame origins, this means that the lower limits that we report for possibly eccentric events are overly conservative for binaries in the source frame. On the flip side, upper limits reported for non-eccentric events are less conservative for source-frame binaries. We convert measurements of eccentricity into the source frame by establishing the source-frame frequency corresponding to a detector-frame frequency of 10 Hz: $f_{\text{source}} = 10(1+z)$ Hz. We then back-evolve e_{10} from $f_{\text{source}} = 10(1+z)$ Hz to $f_{\text{source}} = 10$ Hz using Peter’s equations (Peters 1964).

An additional complication comes from conflicting definitions of the reference frequency at which eccentricity is quoted. The reference frequency of the SEOBNRE model, f_{SEOBNRE} , is defined relative to a closed Keplerian orbit, with a semi-major axis that changes as the binary inspirals. Meanwhile, simulations of cluster mergers report eccentricities defined at the peak frequency of gravitational-wave emission, f_{peak} . Within SEOBNRE, an eccentric correction is applied such that the minimum frequency of gravitational-wave content is $f_{\text{SEOBNRE,min}} = f_{\text{SEOBNRE}}/(1 - e_{\text{SEOBNRE}}^2)^{1.5}$. This means that at $f_{\text{SEOBNRE}} = 10$ Hz, the maximum dif-

ference between f_{SEOBNRE} and $f_{\text{SEOBNRE,min}}$ is 0.63 Hz (for $e_{\text{SEOBNRE}} = 0.2$). We start analysis for most events from 20 Hz, with the exception of GW190521, which we start from 11 Hz. Therefore, this internal eccentric correction does not cause the waveform to start within our analysis band. However, our reported e_{10} measurements are not directly comparable to the predictions of globular cluster simulations, since (Wen 2003)

$$f_{\text{peak}} = f_{\text{SEOBNRE}}(1 - e_{\text{SEOBNRE}}^2)^{-1.5}(1 + e_{\text{SEOBNRE}})^{1.1954}. \quad (3)$$

The maximal difference between f_{SEOBNRE} and f_{peak} is therefore 3.2 Hz (for $e_{\text{SEOBNRE}} = 0.2$).

We convert from an eccentricity distribution defined at $f_{\text{SEOBNRE}} = 10$ Hz in the detector frame to its equivalent at $f_{\text{peak}} = 10$ Hz in the source frame using Eq. 3 and Peter’s equations (Peters 1964). We caution that these results be taken as indicative rather than exact measurements: evolving back to $f_{\text{peak}} = 10$ Hz pushes f_{SEOBNRE} to lower frequencies. Therefore, we are implicitly assuming that the inspiral of the system was unperturbed at lower frequencies, corresponding to earlier times.

In the left-hand panel of Fig. 7, we plot measured median and upper 90% credible intervals on eccentricity at 10 Hz in the detector frame, e_{10} , against source-frame chirp mass \mathcal{M} of the 62 BBH analysed in this work. On the right-hand side, we plot median and upper 90% credible intervals for $e_{10,\text{peak,source}}$, the eccentricity at a peak gravitational-wave frequency of 10 Hz in the source frame, following the conversions described above. The number of binaries with $e_{10,\text{peak,source}} \geq 0.05$ is the same as that with detector-frame eccentricity at 10 Hz Keplerian frequency $e_{10} \geq 0.05$: we find four binaries above this threshold in both cases.

We can now use the fraction of binaries detected with $e_{10} \geq 0.05$ to constrain the fractional presence of mergers produced dense star clusters within the population. Consistent with Zevin et al. (2021a), we call this the branching fraction, B_c . In Fig. 8, we plot in teal the likelihood on B_c calculated following Zevin et al. (2021a), which treats the number of eccentric mergers in the observed population as a Poisson counting problem. The likelihood for detecting four eccentric binaries within 62 mergers is represented by the teal curve, with the grey shaded rectangle indicating the region in which the prior probability goes to zero ($B_c > 1$). Since we still have a small population and many uncertainties from both our method and our theoretical models, we cannot constrain B_c very tightly or confidently at this stage. *If* all four of our eccentric candidates are truly eccentric, and *if* all eccentric mergers are formed within globular clusters, then globular clusters must contribute at least 35% of observed mergers, at 95% credibility (to calculate this we use the posterior, i.e., we ignore parts of the likelihood greater than one).

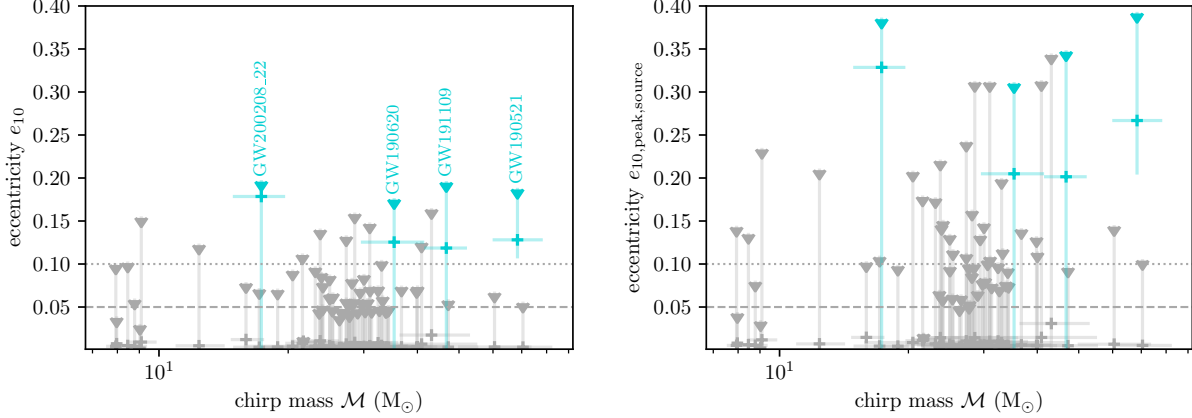


Figure 7. The upper 90% credible limits for all BBH candidates in GWTC-3 are shown as downward-facing triangles, plotted against their median source-frame chirp mass. The panel on the left shows eccentricities as measured at a Keplerian gravitational-wave frequency of 10 Hz in the detector frame, while the right-hand panel shows eccentricities shifted to a peak gravitational-wave frequency of 10 Hz in the source frame. The symmetric 90% credible chirp mass range is indicated for each binary by a horizontal line through their median eccentricity. The median eccentricity is plotted against median source-frame chirp mass with a plus symbol. The four events with more than 50% of their posterior probability distribution above $e_{10} = 0.05$ are highlighted in teal and labelled with their names in the left-hand plot, while all other events are shown in grey. Undersampled events are not plotted.

A population model for the eccentricity distribution

There are multiple pathways that can lead to BBH mergers with detectable eccentricity in the LIGO-Virgo sensitivity band. As the population grows, it may be possible to distinguish mergers from these different channels by studying the shape of the population eccentricity distribution. In Figure 9, we illustrate a simplified population model containing three mechanisms that may produce eccentric mergers with distinct eccentricity distributions: mergers facilitated by interactions within globular cluster mergers (GCS), binary mergers occurring within field triples (TRIPLES), and mergers inside active galactic nuclei (AGN). These populations are represented as follows:

- **GCS:** We represent the distribution shown in Figure 1 of Zevin et al. (2021a) using a Gaussian mixture model containing four Gaussians in $\log_{10}(e_{10})$ at $\mu = [-6.9, -4.9, -1.5, 0]$ with widths $\sigma = [0.5, 1.0, 1.1, 0.1]$. These peaks, respectively, correspond to: mergers that form in clusters and are ejected before they merge; mergers that occur after dynamical interactions within clusters; gravitational-wave capture mergers; and gravitational-wave capture mergers that become bound within the LVK band, merging with eccentricities close to unity.
- **TRIPLES:** Binaries can be driven to merge rapidly in isolation if gravitational energy is removed from their orbit by a third object with which they are bound. In some cases, the eccentricity of these binaries can be amplified through Lidov-Kozai oscillations (e.g., Lidov 1962; Kozai 1962). Following Lower et al. (2018)

and references therein, we model the primary component expected eccentricity distribution from field triples as a single Gaussian in $\log_{10}(e_{10})$ centred at $\mu = -3$ with width $\sigma = 0.7$ for simplicity. We ignore the small higher-eccentricity peak expected for $\sim 5\%$ of field triples since the contribution from this channel is expected to be small (e.g., Silsbee & Tremaine 2017; Rodriguez & Antonini 2018), and we include it in our model for illustrative purposes only (we do not include it in our toy-population-model analyses).

- **AGN:** In the dense centre and accretion disk of an active galactic nucleus, binaries can be driven to merge through dynamical interactions. The eccentricity distribution of dynamical mergers inside AGN differs from that expected in globular clusters because the central gravitational potential of the nucleus is greater, and various interactions can also occur within the accretion disk. The distribution expected from AGN is highly uncertain and depends greatly on the properties of the AGN. With reference to Samsing et al. (2020) (see the right-hand panel of their Figure 5 in particular), we represent the contribution from AGN as a Gaussian in $\log_{10}(e_{10})$ centred at $\mu = -1.2$ and $\sigma = 1.0$. We recognise this as a greatly simplified model, and present this as a proof-of-concept that can be extended to include more complete distributions predicted by complex AGN models.

Inferring the formation mechanisms of binaries should incorporate contributions from multiple different channels, likely many more than are represented in our simple model.

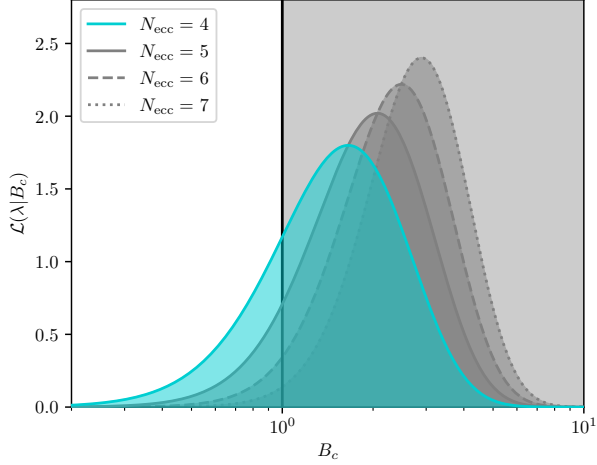


Figure 8. The posterior probability of the branching fraction, B_c , if all eccentric mergers are produced in globular clusters, following the model in Zevin et al. (2021a). We take $N_{\text{obs}} = 62$ as the number of observed events, not counting those that end up undersampled after reweighting. The black line denotes $B_c = 1$, which corresponds to 100% of mergers being formed in globular clusters. Above this line, non-zero likelihood support indicates that there are more eccentric mergers than can be accounted for with globular cluster mergers alone. We plot the probability for $N_{\text{ecc}} = 4$, the number of mergers we find with $e_{10} \geq 0.05$, and for $N_{\text{ecc}} = 5, 6$ and 7 to account for the additional eccentric merger candidates with $\ln B(e_{10} \geq 0.1) > 1$ from GWTC-2 (GW190706A; Romero-Shaw et al. 2021a) and GWTC-3 (GW191126, GW191127). It remains feasible for $\leq 100\%$ of observed mergers to be forming in globular clusters with four eccentric events within the population. However, the peak of the probability lies above the $B_c = 1$ line, indicating that another process may be producing eccentric mergers. Additionally, if many of the candidates with less well-measured eccentricities are truly eccentric, the globular cluster hypothesis becomes less likely.

For the sake of this proof-of-principle demonstration, we generate populations of events from the GCs channel only, approximating each event’s eccentricity posterior probability distribution as a delta function. Since our eccentricity measurements typically have broader posteriors than a delta function, the result of this simple demonstration should be taken as a lower limit. We generate populations ranging in size from 5 to 200 events, and recover the population distribution using the hyper submodule of bilby (Ashton et al. 2019; Romero-Shaw et al. 2020c). We obtain log Bayes factors, $\ln B_{\text{GCs}}$, for the strength of the GC hypothesis relative to the AGN hypothesis, taking $\ln B_{\text{GCs}} \geq 8$ as a “confident” preference for the GC hypothesis. We study only the range of eccentricities that is accessible to each era of detector:

- **LVK sensitivity limit:** Although sensitivity to eccentricity varies slightly with mass (see Appendix C of Romero-Shaw et al. (2021a)), we take $e_{10} \geq 0.05$ as the range within which existing detectors can measure

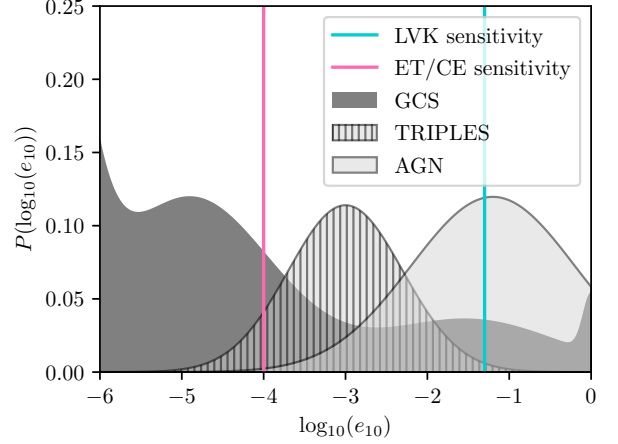


Figure 9. A simplistic toy model for the eccentricity distribution arising as a byproduct of three different formation mechanisms: dynamical mergers in GCs (dark grey) and AGN (light grey), in addition to field triples (striped grey). Each mechanism is represented by either a single Gaussian or a mixture of Gaussians of different weights. The vertical teal line shows the approximate limit of LIGO-Virgo sensitivity to eccentricity at $e_{10} = 0.05$ and the vertical pink line shows the estimated sensitivity of third-generation detectors Einstein Telescope (ET) and Cosmic Explorer (CE) to eccentricity at $e_{10} \approx 10^{-4}$.

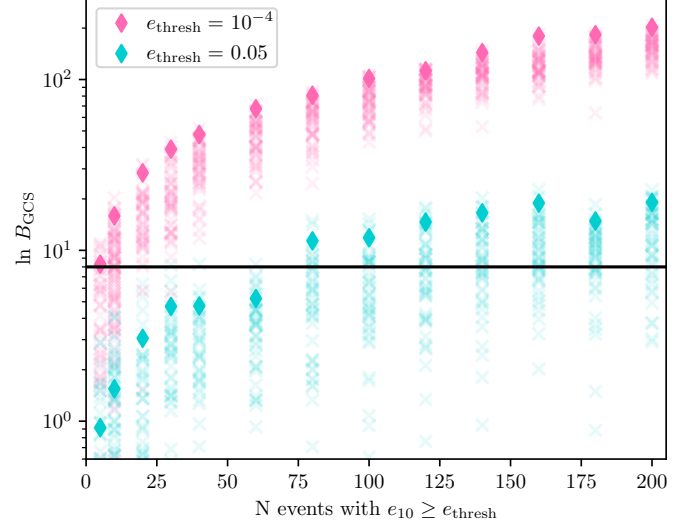


Figure 10. The log Bayes factor $\ln B_{\text{GCs}}$ for the GC hypothesis relative to the AGN hypothesis with N events and studying eccentricities only above e_{thresh} . The two e_{thresh} represent the approximate sensitivity of current detectors ($e_{10} \sim 0.05$) and third-generation detectors ($e_{10} \approx 10^{-4}$). For each N , we calculate $\ln B_{\text{GCs}}$ for 50 mock populations (shown with translucent crosses) and take the average (shown with opaque diamonds). The threshold value of $\ln B_{\text{GCs}}$ for “confident” detection, which we take to be 8 by convention, is represented with a black line.

eccentricity. This is consistent with our own measurements, as well as the predictions of [Lower et al. \(2018\)](#).

- **Einstein Telescope / Cosmic Explorer sensitivity limit:** We use samples from the range of eccentricities to which the Einstein Telescope (ET) and Cosmic Explorer (CE) are expected to be sensitivity; this is approximately $e_{10} \geq 10^{-4}$ ([Lower et al. 2018](#)).

For each N and for each sensitivity threshold, we perform parameter estimation on 50 mock populations. We plot our results in Figure 10, where the average $\ln B_{\text{GCs}}$ for each N obtained is marked with a diamond. We find that we will be able to confidently distinguish a BBH merger population dominated by those formed in GCs from one in which mergers form in AGN with ≥ 80 detectably-eccentric events. This is a lower limit, since real detections have non-negligible uncertainties. Additionally, it will be trickier to disentangle the contributions of multiple channels that contribute comparable numbers of eccentric binaries to the population. We leave a detailed simulation study that accounts for these complications for future work.

CONCLUSION

In this work, we analyse 26 BBH signal candidates from GWTC-3 for signs of orbital eccentricity using an aligned-spin, eccentric waveform model. We find that two of these events have significant support for detectable eccentricity at 10 Hz: GW191109 and GW200208_22. Together with two events from GWTC-2, GW190521 and GW190620 ([Romero-Shaw et al. 2021a](#)), four of the 62 BBH we have studied show significant support for measurable eccentricity. At just over 6%, this is slightly more than the $\sim 4\%$ of mergers that should be expected with detectable eccentricity from GCs ([Zevin et al. 2021a](#)), and may indicate that there are more eccentric mergers in the population than can be explained by dense star clusters alone. However, as we show in Section 4, the difference can be explained by Poisson noise. Additionally, some of these mergers may be spin-precessing binaries that are masquerading as eccentric BBH in our analyses due to our enforced assumption of spin-alignment.

While we cannot say conclusively that these four binaries are eccentric and spin-aligned, our results do show that these signals are consistent with those that contain hints of orbital eccentricity, and are better-fit by eccentric waveforms than they are by quasi-circular waveforms. If they *are* eccentric, and/or have large spin magnitudes and/or spin tilts, then these binaries are difficult to explain through isolated evolution scenarios and add weight to the hypothesis that the BBH detected by the LVK are dynamically formed.

We have focused on the particular dynamical formation environment of dense star clusters in this paper. However, we emphasise that this is due to the robustness of predictions

from this channel, as opposed to any sign that this particular dynamical formation environment is preferred over other dynamical formation environments. In fact, this formation environment may be particularly *unlikely* when other parameters of these systems are considered. Three of the four potentially eccentric events have notably high primary masses, all with median source-frame measurements above the tentative pair-instability supernova mass gap lower limit of $\sim 55 M_{\odot}$ (e.g., [Heger & Woosley 2002](#); [Belczynski et al. 2016](#); [Woosley 2017](#); [Marchant & Moriya 2020](#)) (the exception, GW200208_22, has a median source-frame primary mass of $\sim 25 M_{\odot}$ after reweighting to the eccentric model). The relatively low escape velocities of globular clusters (typically $\lesssim 120 \text{ km s}^{-1}$; [Gnedin et al. 2002](#); [Antonini & Rasio 2016](#); [Baumgardt & Hilker 2018](#)) mean that merger remnants are more often kicked out of the cluster than in environments with deeper central potential wells, such as AGN or nuclear star clusters (e.g., [Antonini & Rasio 2016](#); [Ford & McKernan 2021](#); [Mahapatra et al. 2021](#)). Additionally, because globular clusters undergo mass segregation soon after their formation at high redshift, it is likely that the heaviest binaries merge outside of the observable range of current detectors ([Antonini & Rasio 2016](#); [Romero-Shaw et al. 2021b](#)). To assess the probability of formation in globular clusters relative to the probability of formation in AGN, we would need a multidimensional version of the toy-model analysis demonstrated in Section 4.2 incorporating robust predictions for eccentricity, mass, spin and redshift from these different environments; see, e.g., [Yang et al. \(2019\)](#); [Samsing et al. \(2020\)](#); [McKernan et al. \(2020\)](#); [Tagawa et al. \(2020, 2021c,b\)](#); [Vajpeyi et al. \(2021\)](#); [Gayathri et al. \(2021\)](#) for a range of recent predictions for binary black hole mergers occurring in AGN.

There are many roads to forming merging BBH dynamically, and we show in this paper that in a future when eccentricity can be tightly constrained, it will be possible to disentangle contributing dynamical channels with ≥ 80 detectably-eccentric mergers at current detector sensitivity limits. As detectors improve, the threshold for detectable eccentricity decreases, so fewer detectably-eccentric events are required to distinguish contributions from different dynamical channels. Even so, without a method to confidently measure eccentricity and the full range of spin effects simultaneously, it will not be possible to use the method we have demonstrated to identify the dominant dynamical formation channel. We will therefore turn our focus towards extricating measurements of eccentricity from the restraints of spin-aligned, moderately-spinning waveform models in the future.

ACKNOWLEDGEMENTS

We thank Vijay Varma, Katerina Chatziioannou, Alan Knee, Teagan Clarke, Makai Baker, and attendees of the Niels

Bohr Institute’s Workshop on Black Hole Dynamics for enlightening suggestions, observations, and discussions. We also thank Mike Zevin for his insights on our work and comments on our manuscript. This work is supported through Australian Research Council (ARC) Centre of Excellence CE170100004, and Discovery Project DP220101610. IMR-S acknowledges support received from the Herchel Smith Postdoctoral Fellowship Fund. The authors are grateful for computational resources provided by the LIGO Laboratory and supported by National Science Foundation Grants PHY-0757058 and PHY-0823459. This research has made use of data or software obtained from the Gravitational Wave Open Science Center (gw-openscience.org), a service of LIGO Laboratory, the LIGO Scientific Collaboration, the Virgo Collaboration, and KAGRA. LIGO Laboratory and Advanced LIGO are funded by the United States National Science Foundation (NSF) as well as the Science and Technology Facilities Coun-

cil (STFC) of the United Kingdom, the Max-Planck-Society (MPS), and the State of Niedersachsen/Germany for support of the construction of Advanced LIGO and construction and operation of the GEO600 detector. Additional support for Advanced LIGO was provided by the Australian Research Council. Virgo is funded, through the European Gravitational Observatory (EGO), by the French Centre National de Recherche Scientifique (CNRS), the Italian Istituto Nazionale di Fisica Nucleare (INFN) and the Dutch Nikhef, with contributions by institutions from Belgium, Germany, Greece, Hungary, Ireland, Japan, Monaco, Poland, Portugal, Spain. The construction and operation of KAGRA are funded by Ministry of Education, Culture, Sports, Science and Technology (MEXT), and Japan Society for the Promotion of Science (JSPS), National Research Foundation (NRF) and Ministry of Science and ICT (MSIT) in Korea, Academia Sinica (AS) and the Ministry of Science and Technology (MoST) in Taiwan.

REFERENCES

- Abbott, B. P., et al. 2019, *Phys. Rev. X*, 9, 031040, doi: [10.1103/PhysRevX.9.031040](https://doi.org/10.1103/PhysRevX.9.031040)
- Abbott, R., Abbott, T. D., Acernese, F., et al. 2021a, arXiv e-prints, arXiv:2111.03606. <https://arxiv.org/abs/2111.03606>
- Abbott, R., Abbott, T. D., Abraham, S., et al. 2020, *Phys. Rev. Lett.*, 125, 101102, doi: [10.1103/PhysRevLett.125.101102](https://doi.org/10.1103/PhysRevLett.125.101102)
- Abbott, R., Abbott, T. D., Abraham, S., et al. 2020, *ApJL*, 896, L44, doi: [10.3847/2041-8213/ab960f](https://doi.org/10.3847/2041-8213/ab960f)
- . 2021b, *Physical Review X*, 11, 021053, doi: [10.1103/PhysRevX.11.021053](https://doi.org/10.1103/PhysRevX.11.021053)
- Abbott, R., Abbott, T. D., Acernese, F., et al. 2021c, arXiv e-prints, arXiv:2108.01045. <https://arxiv.org/abs/2108.01045>
- . 2021d, arXiv e-prints, arXiv:2111.03634. <https://arxiv.org/abs/2111.03634>
- Abbott, R., et al. 2021a, Gravitational Wave Open Science Center Strain Data Release for GWTC-2.1, LIGO Open Science Center, doi: <https://doi.org/10.7935/qf3a-3z67>
- . 2021b, Gravitational Wave Open Science Center Strain Data Release for GWTC-3, LIGO Open Science Center, doi: <https://doi.org/10.7935/pr1e-j706>
- Anagnostou, O., Trenti, M., & Melatos, A. 2020, arXiv e-prints, arXiv:2010.06161. <https://arxiv.org/abs/2010.06161>
- Antonini, F., & Rasio, F. A. 2016, *ApJ*, 831, 187, doi: [10.3847/0004-637X/831/2/187](https://doi.org/10.3847/0004-637X/831/2/187)
- Antonini, F., Toonen, S., & Hamers, A. S. 2017, *Astrophys. J.*, 841, 77, doi: [10.3847/1538-4357/aa6f5e](https://doi.org/10.3847/1538-4357/aa6f5e)
- Ashton, G., et al. 2019, *Astrophys. J. Suppl.*, 241, 27, doi: [10.3847/1538-4365/ab06fc](https://doi.org/10.3847/1538-4365/ab06fc)
- Banerjee, S. 2021, *MNRAS*, 500, 3002, doi: [10.1093/mnras/staa2392](https://doi.org/10.1093/mnras/staa2392)
- Baumgardt, H., & Hilker, M. 2018, *MNRAS*, 478, 1520, doi: [10.1093/mnras/sty1057](https://doi.org/10.1093/mnras/sty1057)
- Bavera, S. S., Fragos, T., Qin, Y., et al. 2020, *A&A*, 635, A97, doi: [10.1051/0004-6361/201936204](https://doi.org/10.1051/0004-6361/201936204)
- Belczynski, K. 2020, *ApJL*, 905, L15, doi: [10.3847/2041-8213/abcbl1](https://doi.org/10.3847/2041-8213/abcbl1)
- Belczynski, K., Heger, A., Gladysz, W., et al. 2016, *A&A*, 594, A97, doi: [10.1051/0004-6361/201628980](https://doi.org/10.1051/0004-6361/201628980)
- Belczynski, K., Klencki, J., Fields, C. E., et al. 2020, *A&A*, 636, A104, doi: [10.1051/0004-6361/201936528](https://doi.org/10.1051/0004-6361/201936528)
- Bethe, H. A., & Brown, G. E. 1998, *Astrophys. J.*, 506, 780, doi: [10.1086/306265](https://doi.org/10.1086/306265)
- Bogdanović, T., Reynolds, C. S., & Miller, M. C. 2007, *ApJL*, 661, L147, doi: [10.1086/518769](https://doi.org/10.1086/518769)
- Broekgaarden, F. S., Stevenson, S., & Thrane, E. 2022, arXiv e-prints, arXiv:2205.01693. <https://arxiv.org/abs/2205.01693>
- Buonanno, A., Kidder, L. E., & Lehner, L. 2008, *PhRvD*, 77, 026004, doi: [10.1103/PhysRevD.77.026004](https://doi.org/10.1103/PhysRevD.77.026004)
- Calderón Bustillo, J., Sanchis-Gual, N., Torres-Forné, A., & Font, J. A. 2020, Confusing head-on and precessing intermediate-mass binary black hole mergers
- Calderón Bustillo, J., Sanchis-Gual, N., Torres-Forné, A., et al. 2021, *Phys. Rev. Lett.*, 126, 081101, doi: [10.1103/PhysRevLett.126.081101](https://doi.org/10.1103/PhysRevLett.126.081101)
- Campanelli, M., Lousto, C. O., & Zlochower, Y. 2006, *Phys. Rev. D*, D74, 084023, doi: [10.1103/PhysRevD.74.084023](https://doi.org/10.1103/PhysRevD.74.084023)
- Cao, Z., & Han, W.-B. 2017, *Phys. Rev.*, D96, 044028, doi: [10.1103/PhysRevD.96.044028](https://doi.org/10.1103/PhysRevD.96.044028)
- Clarke, T. A., Romero-Shaw, I. M., Lasky, P. D., & Thrane, E. 2022, arXiv e-prints, arXiv:2206.14006. <https://arxiv.org/abs/2206.14006>

- Cornish, N. J., & Littenberg, T. B. 2015, *Class. Quant. Grav.*, 32, 135012, doi: [10.1088/0264-9381/32/13/135012](https://doi.org/10.1088/0264-9381/32/13/135012)
- Costa, G., Bressan, A., Mapelli, M., et al. 2021, *MNRAS*, 501, 4514, doi: [10.1093/mnras/staa3916](https://doi.org/10.1093/mnras/staa3916)
- de Mink, S. E., Cantiello, M., Langer, N., & Pols, O. R. 2010, in *American Institute of Physics Conference Series*, Vol. 1314, American Institute of Physics Conference Series, ed. V. Kalogera & M. van der Sluys, 291–296, doi: [10.1063/1.3536387](https://doi.org/10.1063/1.3536387)
- de Mink, S. E., & Mandel, I. 2016, *Mon. Not. Roy. Astron. Soc.*, 460, 3545, doi: [10.1093/mnras/stw1219](https://doi.org/10.1093/mnras/stw1219)
- Farmer, R., Renzo, M., de Mink, S. E., Marchant, P., & Justham, S. 2019, *Astrophys. J.*, 887, 53
- Farr, W. M., Stevenson, S., Coleman Miller, M., et al. 2017, *Nature*, 548, 426, doi: [10.1038/nature23453](https://doi.org/10.1038/nature23453)
- Favata, M., Kim, C., Arun, K. G., Kim, J., & Lee, H. W. 2022, *Phys. Rev. D*, 105, 023003, doi: [10.1103/PhysRevD.105.023003](https://doi.org/10.1103/PhysRevD.105.023003)
- Fishbach, M., & Holz, D. E. 2017, *Astrophys. J.*, 851, L25, doi: [10.3847/2041-8213/aa9bf6](https://doi.org/10.3847/2041-8213/aa9bf6)
- Fishbach, M., & Holz, D. E. 2020, arXiv e-prints, arXiv:2009.05472. <https://arxiv.org/abs/2009.05472>
- Fishbach, M., Holz, D. E., & Farr, B. 2017, *Astrophys. J.*, 840, L24, doi: [10.3847/2041-8213/aa7045](https://doi.org/10.3847/2041-8213/aa7045)
- Fishbach, M., Holz, D. E., & Farr, W. M. 2018, *apjl*, 863, L41, doi: [10.3847/2041-8213/aad800](https://doi.org/10.3847/2041-8213/aad800)
- Ford, K. E. S., & McKernan, B. 2021, arXiv e-prints, arXiv:2109.03212. <https://arxiv.org/abs/2109.03212>
- Franciolini, G., Cotesta, R., Loutrel, N., et al. 2021, arXiv e-prints, arXiv:2112.10660. <https://arxiv.org/abs/2112.10660>
- Galaudage, S., Talbot, C., Nagar, T., et al. 2021, arXiv e-prints, arXiv:2109.02424. <https://arxiv.org/abs/2109.02424>
- Gallegos-Garcia, M., Berry, C. P. L., Marchant, P., & Kalogera, V. 2021, *ApJ*, 922, 110, doi: [10.3847/1538-4357/ac2610](https://doi.org/10.3847/1538-4357/ac2610)
- Gayathri, V., Yang, Y., Tagawa, H., Haiman, Z., & Bartos, I. 2021, *ApJL*, 920, L42, doi: [10.3847/2041-8213/ac2cc1](https://doi.org/10.3847/2041-8213/ac2cc1)
- Gayathri, V., Healy, J., Lange, J., et al. 2022, *Nature Astron.*, 6, 344, doi: [10.1038/s41550-021-01568-w](https://doi.org/10.1038/s41550-021-01568-w)
- Gerosa, D., & Berti, E. 2017, *Phys. Rev.*, D95, 124046, doi: [10.1103/PhysRevD.95.124046](https://doi.org/10.1103/PhysRevD.95.124046)
- Gerosa, D., & Berti, E. 2019, *PhRvD*, 100, 041301, doi: [10.1103/PhysRevD.100.041301](https://doi.org/10.1103/PhysRevD.100.041301)
- Gerosa, D., Berti, E., O’Shaughnessy, R., et al. 2018, *Phys. Rev. D*, 98, 084036, doi: [10.1103/PhysRevD.98.084036](https://doi.org/10.1103/PhysRevD.98.084036)
- Gerosa, D., & Fishbach, M. 2021, *Nature Astronomy*, 5, 749, doi: [10.1038/s41550-021-01398-w](https://doi.org/10.1038/s41550-021-01398-w)
- Gnedin, O. Y., Zhao, H., Pringle, J. E., et al. 2002, *ApJL*, 568, L23, doi: [10.1086/340319](https://doi.org/10.1086/340319)
- Gondán, L., & Kocsis, B. 2021, *Mon. Not. Roy. Astron. Soc.*, doi: [10.1093/mnras/stab1722](https://doi.org/10.1093/mnras/stab1722)
- González, J. A., Sperhake, U., Brüggmann, B., Hannam, M., & Husa, S. 2007, *PhRvL*, 98, 091101, doi: [10.1103/PhysRevLett.98.091101](https://doi.org/10.1103/PhysRevLett.98.091101)
- Green, A. M., & Kavanagh, B. J. 2021, *Journal of Physics G Nuclear Physics*, 48, 043001, doi: [10.1088/1361-6471/abc534](https://doi.org/10.1088/1361-6471/abc534)
- Hannam, M., Hoy, C., Thompson, J. E., et al. 2021, arXiv e-prints, arXiv:2112.11300. <https://arxiv.org/abs/2112.11300>
- Heger, A., & Woosley, S. E. 2002, *Astrophys. J.*, 567, 532, doi: [10.1086/338487](https://doi.org/10.1086/338487)
- Hirschi, R., Meynet, G., & Maeder, A. 2005, *A&A*, 443, 581, doi: [10.1051/0004-6361:20053329](https://doi.org/10.1051/0004-6361:20053329)
- Ivanova, N., Justham, S., Chen, X., et al. 2013, *A&A Rv*, 21, 59, doi: [10.1007/s00159-013-0059-2](https://doi.org/10.1007/s00159-013-0059-2)
- Izzard, R. G., Ramirez-Ruiz, E., & Tout, C. A. 2003, *Monthly Notices of the Royal Astronomical Society*, 348, 1215
- Kalogera, V. 2000, *apj*, 541, 319, doi: [10.1086/309400](https://doi.org/10.1086/309400)
- Khan, S., Husa, S., Hannam, M., et al. 2016, *Phys. Rev.*, D93, 044007, doi: [10.1103/PhysRevD.93.044007](https://doi.org/10.1103/PhysRevD.93.044007)
- Kimball, C., Talbot, C., Berry, C. P., et al. 2021, *Astrophys. J. Lett.*, 915, L35
- Kimball, C., Talbot, C., Berry, C. P. L., et al. 2020, arXiv e-prints, arXiv:2005.00023. <https://arxiv.org/abs/2005.00023>
- Knee, A., Romero-Shaw, I. M., Lasky, P. D., Thrane, E., & McIver, J. 2022, A "Rosetta Stone" to translate between eccentricity in different waveform models
- Kozai, Y. 1962, *Astrophys. J.*, 67, 591, doi: [10.1086/108790](https://doi.org/10.1086/108790)
- Kremer, K., Spera, M., Becker, D., et al. 2020a, *ApJ*, 903, 45, doi: [10.3847/1538-4357/abb945](https://doi.org/10.3847/1538-4357/abb945)
- Kremer, K., Ye, C. S., Rui, N. Z., et al. 2020b, *apjs*, 247, 48, doi: [10.3847/1538-4365/ab7919](https://doi.org/10.3847/1538-4365/ab7919)
- Kruckow, M. U., Tauris, T. M., Langer, N., et al. 2016, *Astron. Astrophys.*, 596, A58, doi: [10.1051/0004-6361/201629420](https://doi.org/10.1051/0004-6361/201629420)
- Lenon, A. K., Nitz, A. H., & Brown, D. A. 2020, *MNRAS*, 497, 1966, doi: [10.1093/mnras/staa2120](https://doi.org/10.1093/mnras/staa2120)
- Lidov, M. L. 1962, *Planetary and Space Science*, 9, 719, doi: [10.1016/0032-0633\(62\)90129-0](https://doi.org/10.1016/0032-0633(62)90129-0)
- Littenberg, T. B., & Cornish, N. J. 2015, *Phys. Rev. D*, 91, 084034, doi: [10.1103/PhysRevD.91.084034](https://doi.org/10.1103/PhysRevD.91.084034)
- Liu, B., & Lai, D. 2017, *ApJL*, 846, L11, doi: [10.3847/2041-8213/aa8727](https://doi.org/10.3847/2041-8213/aa8727)
- Livio, M., & Soker, N. 1988, *Astrophys. J.*, 329, 764, doi: [10.1086/166419](https://doi.org/10.1086/166419)
- Lower, M., et al. 2018, *Phys. Rev. D*, 98, doi: [10.1103/PhysRevD.98.083028](https://doi.org/10.1103/PhysRevD.98.083028)
- Mahapatra, P., Gupta, A., Favata, M., Arun, K. G., & Sathyaprakash, B. S. 2021, *ApJL*, 918, L31, doi: [10.3847/2041-8213/ac20db](https://doi.org/10.3847/2041-8213/ac20db)
- Mandel, I., & de Mink, S. E. 2016, *MNRAS*, 458, 2634, doi: [10.1093/mnras/stw379](https://doi.org/10.1093/mnras/stw379)

- Mandic, V., Bird, S., & Cholis, I. 2016, *Phys. Rev. Lett.*, 117, 201102, doi: [10.1103/PhysRevLett.117.201102](https://doi.org/10.1103/PhysRevLett.117.201102)
- Mapelli, M. 2020, *Frontiers in Astronomy and Space Sciences*, 7, 38, doi: [10.3389/fspas.2020.00038](https://doi.org/10.3389/fspas.2020.00038)
- Marchant, P., Langer, N., Podsiadlowski, P., Tauris, T. M., & Moriya, T. J. 2016, *A&A*, 588, A50, doi: [10.1051/0004-6361/201628133](https://doi.org/10.1051/0004-6361/201628133)
- Marchant, P., & Moriya, T. J. 2020, *A&A*, 640, L18, doi: [10.1051/0004-6361/202038902](https://doi.org/10.1051/0004-6361/202038902)
- McKernan, B., Ford, K. E. S., O’Shaughnessy, R., & Wysocki, D. 2020, *MNRAS*, 494, 1203, doi: [10.1093/mnras/staa740](https://doi.org/10.1093/mnras/staa740)
- Nagar, A., et al. 2018, *Phys. Rev. D*, 98, 104052, doi: [10.1103/PhysRevD.98.104052](https://doi.org/10.1103/PhysRevD.98.104052)
- Naoz, S. 2016, *ARA&A*, 54, 441, doi: [10.1146/annurev-astro-081915-023315](https://doi.org/10.1146/annurev-astro-081915-023315)
- Neijssel, C. J., Vinciguerra, S., Vigna-Gómez, A., et al. 2021, *ApJ*, 908, 118, doi: [10.3847/1538-4357/abde4a](https://doi.org/10.3847/1538-4357/abde4a)
- Neijssel, C. J., Vigna-Gómez, A., Stevenson, S., et al. 2019, *MNRAS*, 490, 3740, doi: [10.1093/mnras/stz2840](https://doi.org/10.1093/mnras/stz2840)
- Olejak, A., Belczynski, K., & Ivanova, N. 2021, *A&A*, 651, A100, doi: [10.1051/0004-6361/202140520](https://doi.org/10.1051/0004-6361/202140520)
- O’Shaughnessy, R., Gerosa, D., & Wysocki, D. 2017, *PhRvL*, 119, 011101, doi: [10.1103/PhysRevLett.119.011101](https://doi.org/10.1103/PhysRevLett.119.011101)
- O’Shea, E., & Kumar, P. 2021, arXiv e-prints, arXiv:2107.07981. <https://arxiv.org/abs/2107.07981>
- Payne, E., Hourihane, S., Golomb, J., et al. 2022, arXiv e-prints, arXiv:2206.11932. <https://arxiv.org/abs/2206.11932>
- Payne, E., Talbot, C., & Thrane, E. 2019, *Phys. Rev. D*, 100, 123017, doi: [10.1103/PhysRevD.100.123017](https://doi.org/10.1103/PhysRevD.100.123017)
- Peters, P. C. 1964, *Phys. Rev.*, 136, B1224, doi: [10.1103/PhysRev.136.B1224](https://doi.org/10.1103/PhysRev.136.B1224)
- Pratten, G., García-Quirós, C., Colleoni, M., et al. 2021, *PhRvD*, 103, 104056, doi: [10.1103/PhysRevD.103.104056](https://doi.org/10.1103/PhysRevD.103.104056)
- Pretorius, F. 2005, *PhRvL*, 95, 121101, doi: [10.1103/PhysRevLett.95.121101](https://doi.org/10.1103/PhysRevLett.95.121101)
- Qin, Y., Marchant, P., Fragos, T., Meynet, G., & Kalogera, V. 2019, *ApJL*, 870, L18, doi: [10.3847/2041-8213/aaf97b](https://doi.org/10.3847/2041-8213/aaf97b)
- Rodriguez, C. L., Amaro-Seoane, P., Chatterjee, S., et al. 2018a, *Phys. Rev.*, D98, 123005, doi: [10.1103/PhysRevD.98.123005](https://doi.org/10.1103/PhysRevD.98.123005)
- Rodriguez, C. L., Amaro-Seoane, P., Chatterjee, S., & Rasio, F. A. 2018b, *Phys. Rev. Lett.*, 120, 151101, doi: [10.1103/PhysRevLett.120.151101](https://doi.org/10.1103/PhysRevLett.120.151101)
- Rodriguez, C. L., & Antonini, F. 2018, *ApJ*, 863, 7, doi: [10.3847/1538-4357/aacea4](https://doi.org/10.3847/1538-4357/aacea4)
- Rodriguez, C. L., Zevin, M., Amaro-Seoane, P., et al. 2019, *PhRvD*, 100, 043027, doi: [10.1103/PhysRevD.100.043027](https://doi.org/10.1103/PhysRevD.100.043027)
- Rodriguez, C. L., Zevin, M., Pankow, C., Kalogera, V., & Rasio, F. A. 2016, *Astrophys. J.*, 832, L2, doi: [10.3847/2041-8205/832/1/L2](https://doi.org/10.3847/2041-8205/832/1/L2)
- Romero-Shaw, I., Lasky, P. D., & Thrane, E. 2021a, *ApJL*, 921, L31, doi: [10.3847/2041-8213/ac3138](https://doi.org/10.3847/2041-8213/ac3138)
- Romero-Shaw, I. M., Farrow, N., Stevenson, S., Thrane, E., & Zhu, X.-J. 2020a, *Mon. Not. Roy. Astron. Soc.*, 496, L64, doi: [10.1093/mnras/slaa084](https://doi.org/10.1093/mnras/slaa084)
- Romero-Shaw, I. M., Kremer, K., Lasky, P. D., Thrane, E., & Samsing, J. 2021b, *MNRAS*, 506, 2362, doi: [10.1093/mnras/stab1815](https://doi.org/10.1093/mnras/stab1815)
- Romero-Shaw, I. M., Lasky, P. D., & Thrane, E. 2019, *Mon. Not. Roy. Astron. Soc.*, 490, 5210, doi: [10.1093/mnras/stz2996](https://doi.org/10.1093/mnras/stz2996)
- Romero-Shaw, I. M., Lasky, P. D., Thrane, E., & Bustillo, J. C. 2020b, *Astrophys. J. Lett.*, 903, L5, doi: [10.3847/2041-8213/abbe26](https://doi.org/10.3847/2041-8213/abbe26)
- Romero-Shaw, I. M., et al. 2020c, *Mon. Not. Roy. Astron. Soc.*, 499, 3295, doi: [10.1093/mnras/staa2850](https://doi.org/10.1093/mnras/staa2850)
- Roulet, J., Chia, H. S., Olsen, S., et al. 2021, *Physical Review D*, 104, 083010, doi: [10.1103/PhysRevD.104.083010](https://doi.org/10.1103/PhysRevD.104.083010)
- Sakstein, J., Croon, D., McDermott, S. D., Straight, M. C., & Baxter, E. J. 2020, arXiv e-prints, arXiv:2009.01213. <https://arxiv.org/abs/2009.01213>
- Samsing, J. 2018, *Phys. Rev. D*, D97, 103014, doi: [10.1103/PhysRevD.97.103014](https://doi.org/10.1103/PhysRevD.97.103014)
- Samsing, J., & D’Orazio, D. J. 2018, *Mon. Not. Roy. Astron. Soc.*, 481, doi: [10.1093/mnras/sty2334](https://doi.org/10.1093/mnras/sty2334)
- Samsing, J., D’Orazio, D. J., Askar, A., & Giersz, M. 2018, arXiv e-prints, arXiv:1802.08654. <https://arxiv.org/abs/1802.08654>
- Samsing, J., & Hotokezaka, K. 2020, arXiv e-prints, arXiv:2006.09744. <https://arxiv.org/abs/2006.09744>
- Samsing, J., & Ramirez-Ruiz, E. 2017, *Astrophys. J.*, 840, L14, doi: [10.3847/2041-8213/aa6f0b](https://doi.org/10.3847/2041-8213/aa6f0b)
- Samsing, J., Bartos, I., D’Orazio, D. J., et al. 2020, arXiv e-prints, arXiv:2010.09765. <https://arxiv.org/abs/2010.09765>
- Sedda, M. A., Mapelli, M., Spera, M., Benacquista, M., & Giacobbo, N. 2020, *Astrophys. J.*, 894, 133, doi: [10.3847/1538-4357/ab88b2](https://doi.org/10.3847/1538-4357/ab88b2)
- Silber, K., & Tremaine, S. 2017, *Astrophys. J.*, 836, 39, doi: [10.3847/1538-4357/aa5729](https://doi.org/10.3847/1538-4357/aa5729)
- Speagle, J. S. 2019, arXiv e-prints, arXiv:1904.02180. <https://arxiv.org/abs/1904.02180>
- Stevenson, S., Berry, C. P. L., & Mandel, I. 2017, *Mon. Not. Roy. Astron. Soc.*, 471, 2801, doi: [10.1093/mnras/stx1764](https://doi.org/10.1093/mnras/stx1764)
- Stevenson, S., Ohme, F., & Fairhurst, S. 2015, *Astrophys. J.*, 810, 58, doi: [10.1088/0004-637X/810/1/58](https://doi.org/10.1088/0004-637X/810/1/58)
- Tagawa, H., Haiman, Z., Bartos, I., & Kocsis, B. 2020, *Astrophys. J.*, 899, 26, doi: [10.3847/1538-4357/aba2cc](https://doi.org/10.3847/1538-4357/aba2cc)
- Tagawa, H., Haiman, Z., Bartos, I., Kocsis, B., & Omukai, K. 2021a, *MNRAS*, 507, 3362, doi: [10.1093/mnras/stab2315](https://doi.org/10.1093/mnras/stab2315)
- Tagawa, H., Kocsis, B., Haiman, Z., et al. 2021b, *Astrophys. J. Lett.*, 907, L20, doi: [10.3847/2041-8213/abd4d3](https://doi.org/10.3847/2041-8213/abd4d3)
- . 2021c, *ApJ*, 908, 194, doi: [10.3847/1538-4357/abd555](https://doi.org/10.3847/1538-4357/abd555)

- Talbot, C., & Thrane, E. 2017, *Phys. Rev. D*, 96, 023012
- Trani, A. A., Tanikawa, A., Fujii, M. S., Leigh, N. W. C., & Kumamoto, J. 2021, *MNRAS*, 504, 910, doi: [10.1093/mnras/stab967](https://doi.org/10.1093/mnras/stab967)
- Vajpeyi, A., Thrane, E., Smith, R., McKernan, B., & Ford, K. E. S. 2021, arXiv e-prints, arXiv:2111.03992. <https://arxiv.org/abs/2111.03992>
- Valsecchi, F., Glebbeek, E., Farr, W. M., et al. 2010, *Nature*, 468, 77, doi: [10.1038/nature09463](https://doi.org/10.1038/nature09463)
- van den Heuvel, E. P. J., Portegies Zwart, S. F., & de Mink, S. E. 2017, *MNRAS*, 471, 4256, doi: [10.1093/mnras/stx1430](https://doi.org/10.1093/mnras/stx1430)
- Vitale, S., Lynch, R., Sturani, R., & Graff, P. 2017, *Class. Quant. Grav.*, 34, 03LT01, doi: [10.1088/1361-6382/aa552e](https://doi.org/10.1088/1361-6382/aa552e)
- Wen, L. 2003, *Astrophys. J.*, 598, 419, doi: [10.1086/378794](https://doi.org/10.1086/378794)
- Woosley, S. E. 2017, *apj*, 836, 244, doi: [10.3847/1538-4357/836/2/244](https://doi.org/10.3847/1538-4357/836/2/244)
- Woosley, S. E., & Heger, A. 2021, *ApJL*, 912, L31, doi: [10.3847/2041-8213/abf2c4](https://doi.org/10.3847/2041-8213/abf2c4)
- Yang, Y., Bartos, I., Gayathri, V., et al. 2019, *PhRvL*, 123, 181101, doi: [10.1103/PhysRevLett.123.181101](https://doi.org/10.1103/PhysRevLett.123.181101)
- Zevin, M., & Bavera, S. S. 2022, arXiv e-prints, arXiv:2203.02515. <https://arxiv.org/abs/2203.02515>
- Zevin, M., & Holz, D. E. 2022, arXiv e-prints, arXiv:2205.08549. <https://arxiv.org/abs/2205.08549>
- Zevin, M., Romero-Shaw, I. M., Kremer, K., Thrane, E., & Lasky, P. D. 2021a, arXiv e-prints, arXiv:2106.09042. <https://arxiv.org/abs/2106.09042>
- Zevin, M., Samsing, J., Rodriguez, C., Haster, C.-J., & Ramirez-Ruiz, E. 2019, *Astrophys. J.*, 871, 91, doi: [10.3847/1538-4357/aaf6ec](https://doi.org/10.3847/1538-4357/aaf6ec)
- Zevin, M., Bavera, S. S., Berry, C. P. L., et al. 2021b, *apj*, 910, 152, doi: [10.3847/1538-4357/abe40e](https://doi.org/10.3847/1538-4357/abe40e)
- Ziegler, J., & Freese, K. 2021, *Phys. Rev. D*, 104, 043015, doi: [10.1103/PhysRevD.104.043015](https://doi.org/10.1103/PhysRevD.104.043015)

Table 3. A summary of the detector-frame eccentricity measurements for events in GWTC-3 with negligible support for the hypothesis that $e_{10} \geq 0.05$. Columns are as described in the caption for Table 1.

Event name	$e_{10} \geq 0.1$ (%)	$e_{10} \geq 0.05$ (%)	$\ln \mathcal{B}(e_{10} \geq 0.1)$	$\ln \mathcal{B}(e_{10} \geq 0.05)$	n_{eff}
GW190426_16	3.25	10.69	−0.86	−0.54	1170
GW190916	4.55	11.71	−0.59	−0.35	573
GW190926	6.75	15.61	−0.15	−0.10	42171
GW191103	9.20	17.82	−0.14	−0.09	175
GW191222	0.00	9.40	−1.68	−0.96	118
GW191230	6.75	14.35	−0.46	−0.34	10661
GW200112	0.77	7.94	−0.88	−0.50	39271
GW200128	2.66	11.60	−0.83	−0.36	11755
GW200208	3.57	11.86	−0.70	−0.42	53832
GW200219	3.50	11.53	−0.74	−0.43	36630
GW200220_O6	4.19	13.16	−0.57	−0.31	20910
GW200220_12	7.47	16.20	−0.26	−0.14	13586
GW200224	4.34	16.17	−0.52	−0.03	38653
GW200302	2.44	9.15	−1.08	−0.38	164
GW200306	5.73	14.18	−0.44	−0.25	4995
GW200308	7.60	16.24	−0.03	−0.03	672
GW200311	0.78	6.70	−1.61	−0.83	51442
GW200316	0.77	18.46	−0.67	−0.02	131

APPENDIX

A. LIKELY NON-ECCENTRIC EVENTS FROM GWTC-3

In Table 3, we provide summary statistics for the events from GWTC-3 that are both adequately sampled and have $\ln \mathcal{B}(e_{10} \geq 0.05) < 0$. Marginal posterior distributions on $\log_{10}(e_{10})$ are displayed in Figure 11. Full posterior distributions on all parameters of these events are provided online.⁶

B. UNDERSAMPLED EVENTS FROM GWTC-3

We consider any event with $n_{\text{eff}} < 100$ to be undersampled. With such few samples, measurements can be misleading. We nonetheless include our results for these events in Table 4 for future reference.

When an event is undersampled, it can be informative to study a scatter plot of weights versus eccentricities to gain an understanding of the reason for undersampling. Three examples are shown in Figure 12, in which the n_{eff} (see Eq. 1) dominating samples are highlighted. Firstly, the locations of the scatter points across the eccentricity range are informative: if the event has no support at all for high eccentricities, it will not be possible for highly-eccentric samples to be drawn, so there will be no scatter points at high eccentricities. Secondly, the distribution of weights across the eccentricity range is informative. If highly-weighted samples are spread evenly across the range of eccentricities—as is the case for our first two examples—waveform systematics are

⁶github.com/IsobelMarguarethe/eccentric-GWTC-3

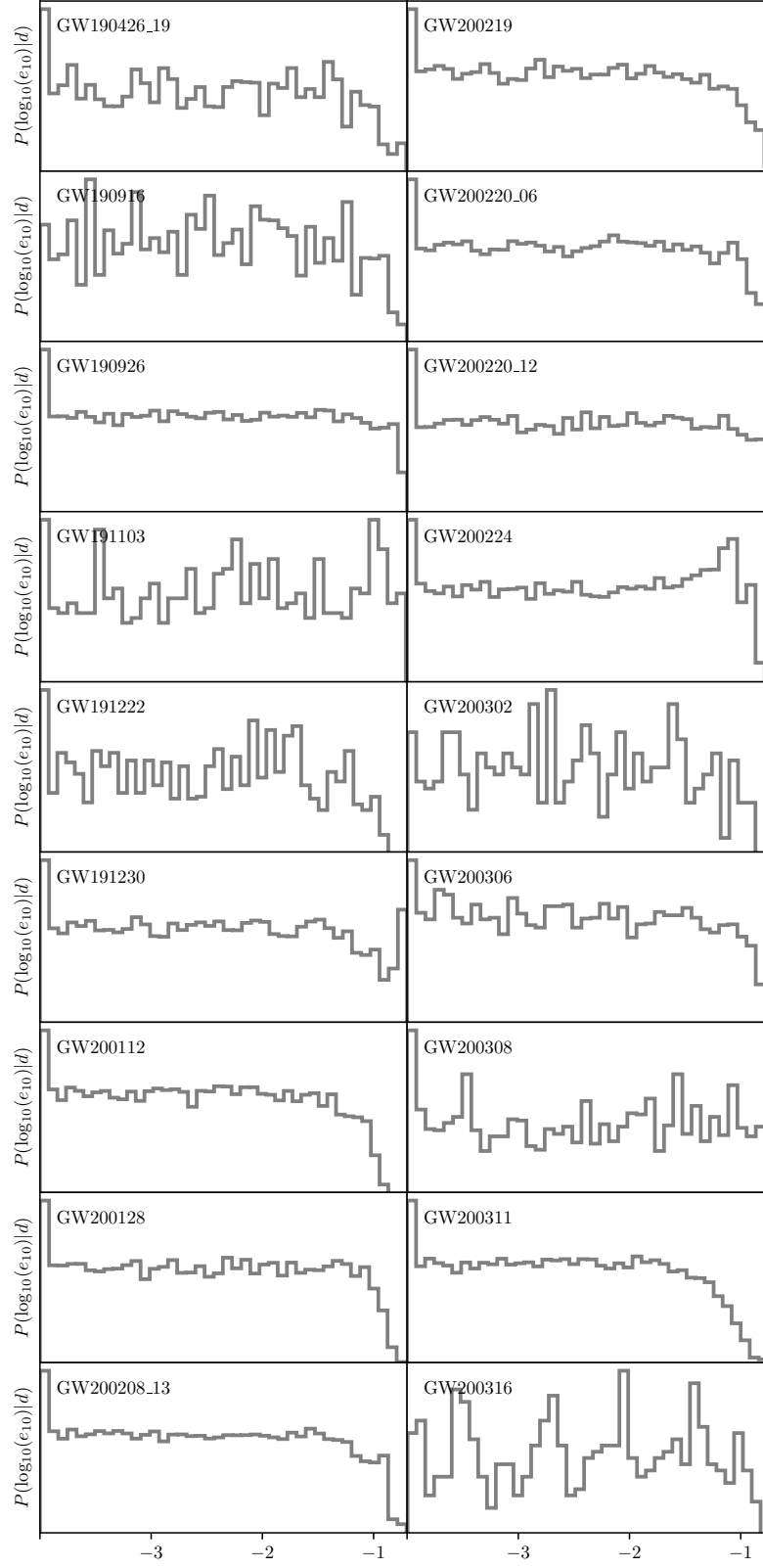


Figure 11. Marginal posterior distributions on $\log_{10}(e_{10})$ for events in GWTC-3 that have negligible support for $e_{10} \geq 0.05$. We label each panel with the name of the event.

Table 4. A summary of the detector-frame eccentricity measurements for events in GWTC-3 that have fewer than 100 effective samples. Columns are as described in the caption for Table 1. Event names with an asterisk are those that were originally reported in GWTC-2, which were undersampled in our analysis of eccentricity in GWTC-2 and were re-analysed for this paper.

Event name	$e_{10} \geq 0.1$ (%)	$e_{10} \geq 0.05$ (%)	$\ln \mathcal{B}(e_{10} \geq 0.1)$	$\ln \mathcal{B}(e_{10} \geq 0.05)$	n_{eff}
<i>GW190412*</i>	0.00	0.00	−5.12	−3.40	3
<i>GW190512*</i>	0.00	6.25	−1.93	−0.73	17
<i>GW190630*</i>	9.09	16.67	0.06	0.00	67
<i>GW190707*</i>	42.86	42.86	1.86	1.10	8
<i>GW190708*</i>	0.00	0.00	−2.19	−2.35	5
<i>GW190720*</i>	23.53	29.41	0.60	0.15	18
<i>GW190725</i>	7.69	53.85	−0.87	1.13	14
<i>GW190728*</i>	0.00	0.00	−1.10	−0.98	14
<i>GW190828_065*</i>	9.09	9.09	0.07	0.97	11
<i>GW190924*</i>	12.50	31.25	−0.71	−0.21	17
<i>GW190925</i>	19.35	35.48	0.72	0.52	32
<i>GW190930*</i>	6.67	26.67	0.40	0.42	15
<i>GW191113</i>	18.42	23.68	0.01	−0.10	39
<i>GW191129</i>	8.16	14.29	−0.52	−0.42	49
<i>GW191204_11</i>	7.04	25.35	−0.24	0.30	71
<i>GW191204_17</i>	33.33	33.33	1.56	0.89	7
<i>GW191215</i>	9.09	29.09	0.00	0.47	55
<i>GW191216</i>	0.00	100.00	−5.11	3.89	1
<i>GW200129</i>	100.00	100.00	10.89	15.41	1
<i>GW200202</i>	3.64	16.36	−0.06	0.52	56
<i>GW200225</i>	42.86	57.14	0.77	0.50	7

a probable suspect for underweighting: these samples are likely to reside in an area of the wider parameter space (for example, a particular combination of masses and spins) for which the IMRPhenomD waveform does not well-represent the $e_{10} = 0$ SEOBNRE waveform. If instead the dominating samples are localised to a particular part of the eccentricity range—as is the case for our final example, GW200129A—the situation is both more interesting and more frustrating. In this case, it is likely that there is strong support for eccentricity in the data, but that the eccentric posterior does not overlap the quasi-circular posterior to an adequate extent for the reweighting method to be efficient.

C. RESULTS FOR BINARIES CONTAINING ONE BLACK HOLE WITH ONE COMPANION THAT MAY BE A NEUTRON STAR OR A BLACK HOLE

In Figures 13 and 14, we present intrinsic and extrinsic parameters inferred for potential NSBH candidates GW190917 and GW200210 under our default priors, which do not extend to the more extreme mass ratios at which these events are known to have the majority of their posterior support. Both events show significant railing at the lower limit of the q prior at 0.125, as well as at the lower limit of the χ_1 and χ_2 priors at -0.6 . While the posteriors on $\log_{10}(e_{10})$ are therefore not to be trusted, and are in any case uninformative, it is interesting to note that the posterior distributions on phase ϕ are informative after reweighting for

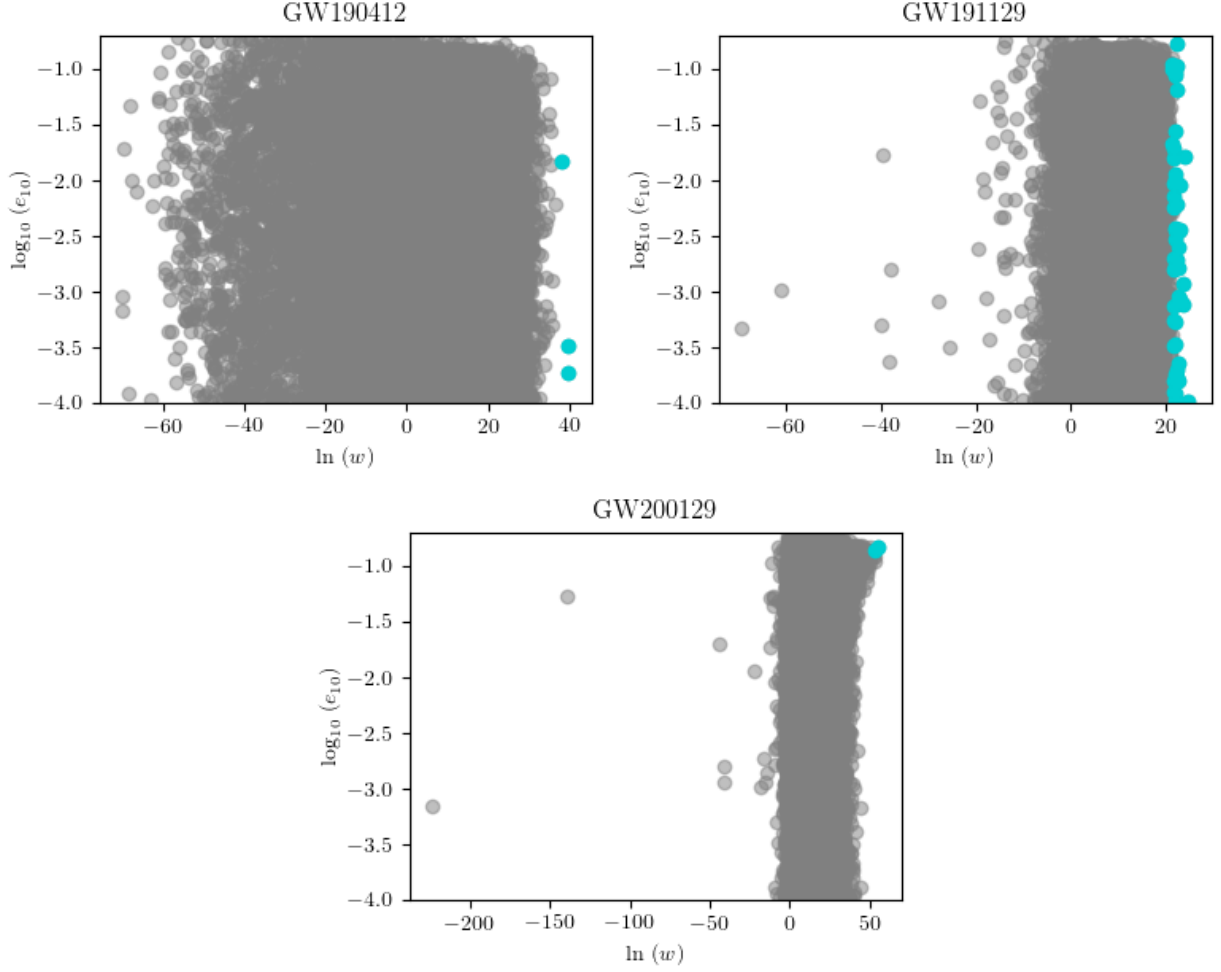


Figure 12. Scatter plots of natural log weight against $\log_{10}(e_{10})$ for three example undersampled events. We label each panel with the name of the event. In each plot, the n_{eff} most highly-weighted samples are highlighted as teal dots. These dots are the points that dominate the reweighted posterior. By plotting the weights against eccentricity in this way, we can see trends that hint at the reason for undersampling. GW190412 and GW191129 (top and middle) have highly-weighted samples spread across the entirety of the eccentricity range, and have relatively low weights for highly-eccentric samples. This hints at waveform systematics being the root of undersampling; if we removed the n_{eff} most highly-weighted samples from these distributions, the resulting posterior on eccentricity would be mostly uninformative, with decreasing support above $e_{10} \approx 0.1$. Meanwhile, the plot for GW200129 (bottom) shows an overall trend towards higher weights for higher eccentricities. If we removed the most highly-weighted sample from this distribution, the posterior would still be undersampled, with the most highly-weighted sample remaining above $e_{10} = 0.1$. To obtain a well-sampled posterior, we would need to remove most of the samples at high eccentricities, hinting that there is strong support for eccentricity in the data and that the eccentric posterior does not have enough overlap with the quasi-circular posterior for the former to be well-sampled using the reweighting method.

both events. The higher-probability peaks correlate with the negative χ_1 peaks: there are only some values of ϕ in those peaks that have high probability density.

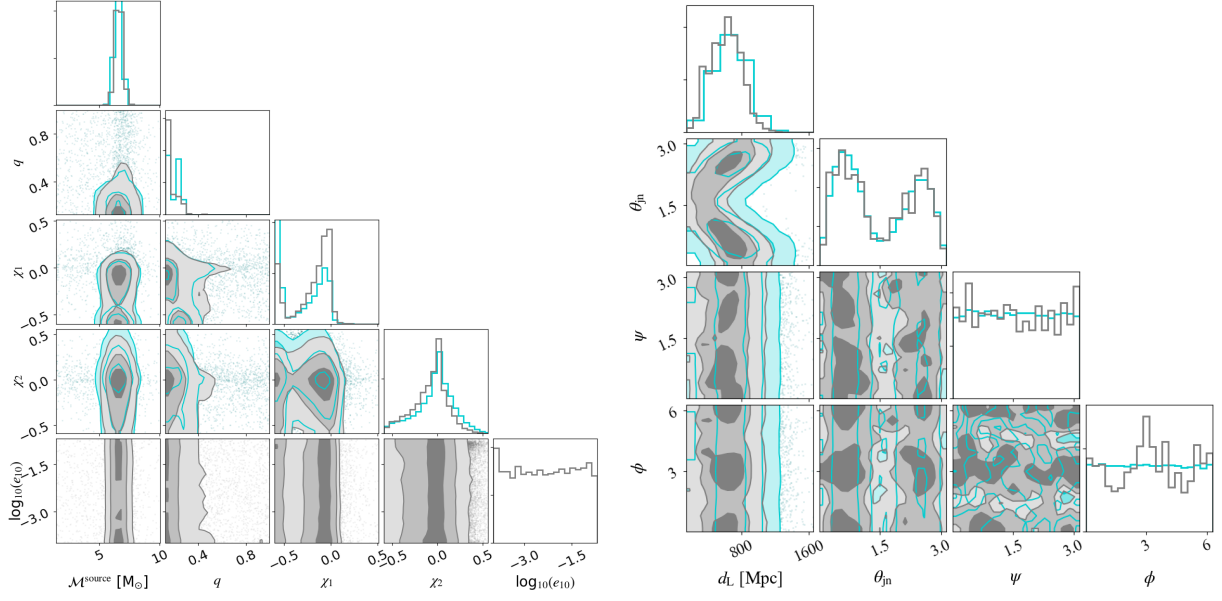


Figure 13. Intrinsic (left) and extrinsic (right) parameters inferred for GW190917. Prior railing can be seen in mass ratio q and both component spin parameters χ_1 and χ_2 .

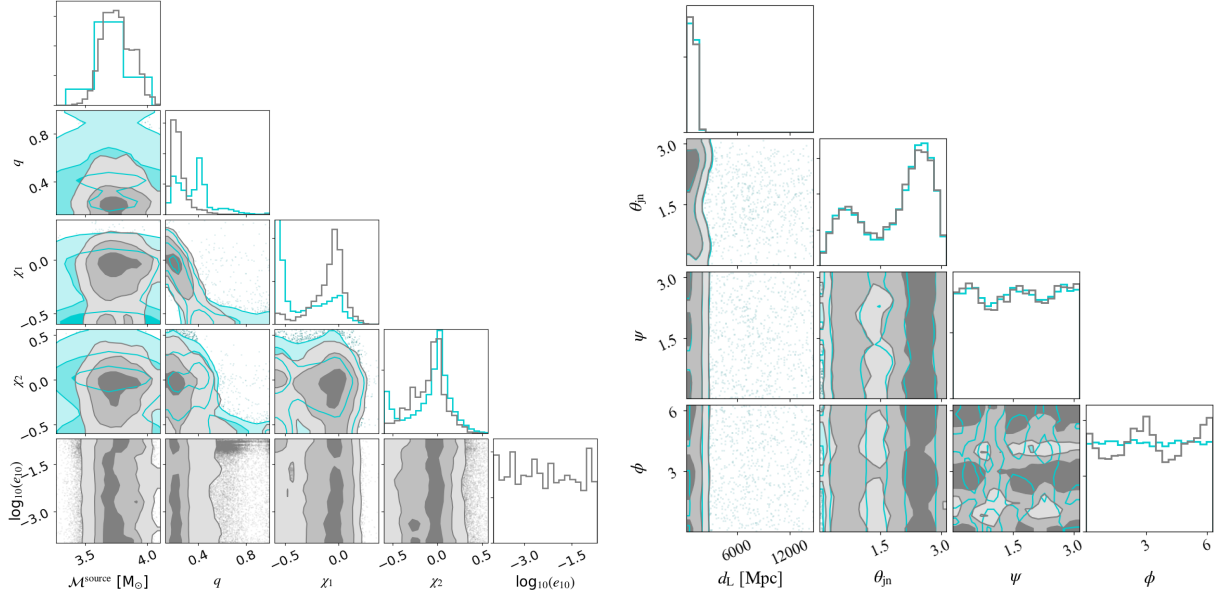


Figure 14. Intrinsic (left) and extrinsic (right) parameters inferred for GW200210. Strong prior railing is evident for mass ratio q and primary component spin parameter χ_1 .